CHAPTER 5

HYDROLOGY AND REGIONAL CHANGES OF THE ISLANDS

5.1 Rainfall characteristics

In the south-western Sundarban, especially in the coastal islands, the chief source of freshwater is rainfall. Most of the rainfall is caused by the south-western monsoon occurring between middle June and middle October yearly. To analyze the rainfall characteristics in this region and the two islands, daily weather data over a 20 year period from 2000 to 2019 were collected. In this section, the temporal trend analysis of yearly rainfall, seasonal rainfall and monthly rainfall are demonstrated. The south-western Sundarban, being a completely flat area of moderate size, experiences almost no spatial variation of climate. The two islands in this study have identical climate due to being so close to each other. So, the climate analysis presented in this chapter is applicable for the south-western Sundarban in general and the islands in particular.

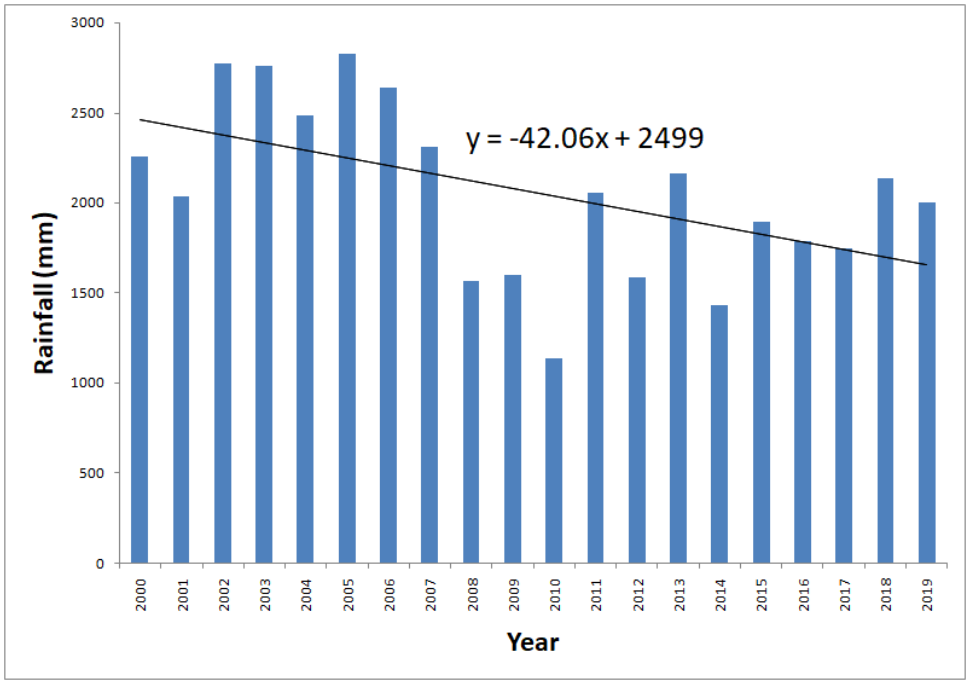

Figure 5.1: Yearly rainfall (2000–2019); station: Diamond Harbour.

The average yearly rainfall over the 20-year period from 2000 to 2019 was found to be 2057.47 mm. The highest rainfall in this period occurred in 2005 (2822.56 mm) and the lowest rainfall happened in 2010 (1135.60 mm). In Figure 5.1, the bar graph of the yearly rainfall is presented along with its linear trend line and its equation. In the equation of the trend line, the y value is the value of the rainfall and the x value is the rank of the year in this series. For example, for the year 2000, $x = 1$, for 2001, $x = 2$, and so on. The negative slope of the trend line clearly convey the declining trend of rainfall in this region. Though the yearly rainfall is

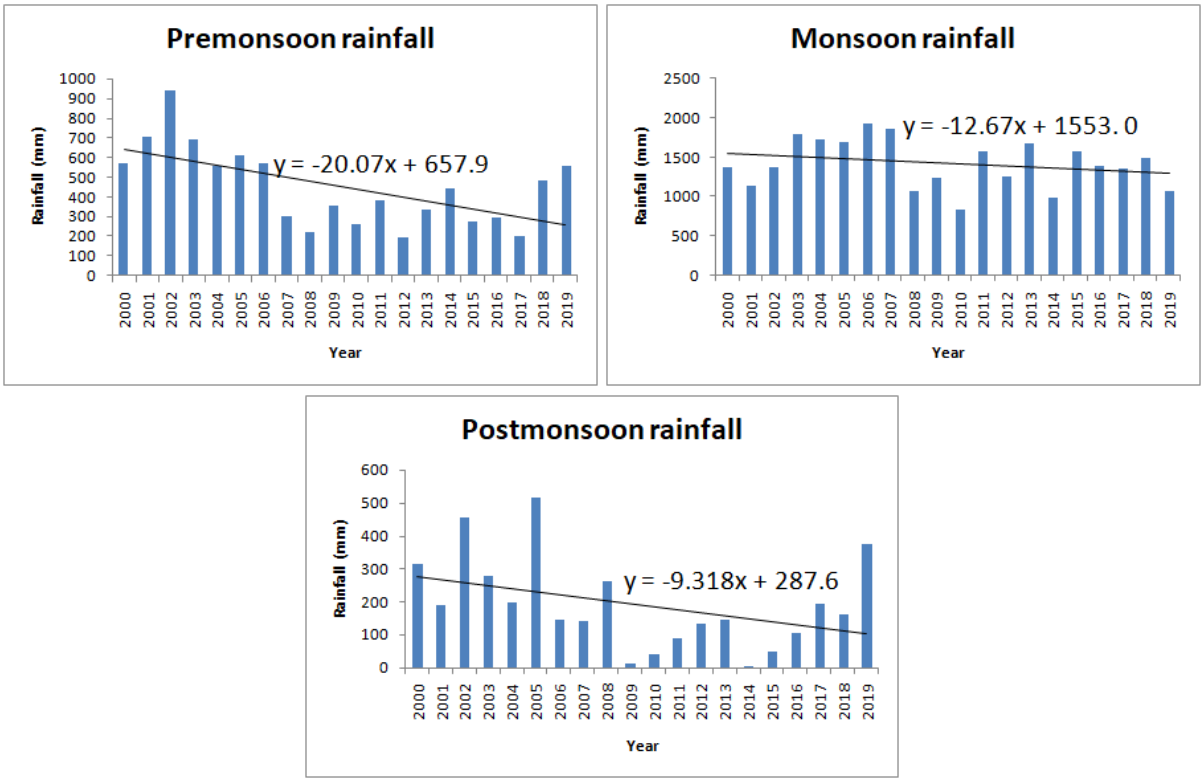

Figure 5.2: Seasonal rainfall (2000–2019); station: Diamond Harbour.

in overall decline, some spans of years had lower rainfall than the estimated trend, while some other spans had higher rainfall. For example, the span from 2002 to 2007 had higher rainfall than the overall trend. On the other hand, the span from 2008 to 2010 had substantially lower rainfall than the linear trend. Rainfall displays an oscillating character between 2011 and 2015 of alternate lower values than the trend and reaching again the trend values.

While the yearly rainfall exhibits a decreasing trend, it is of importance to analyze the season rainfall separately. Because it is the seasonal rainfall, and in particular the monsoonal rainfall, that has a profound effect on the mangrove ecology and certain aspects of the geomorphic features. The seasonal rainfall is analyzed by dividing a year in three seasons: the pre-monsoon, the monsoon and the post-monsoon. The pre-monsoon season is considered fro February 15 to June 14, the monsoon season is taken from June 15 to October 15, and the post-monsoon season is considered from October 16 to December 31 and from January 1 to February 14. Such disconnected formation of the post-monsoon season in a year is required due to the nature of a complete seasonal cycle of the climate.

In Figure 5.2, the seasonal rainfalls over the 20-year time period under consider are presented. It can be seen that in each of the seasons, there is a decreasing trend in rainfall. However, the

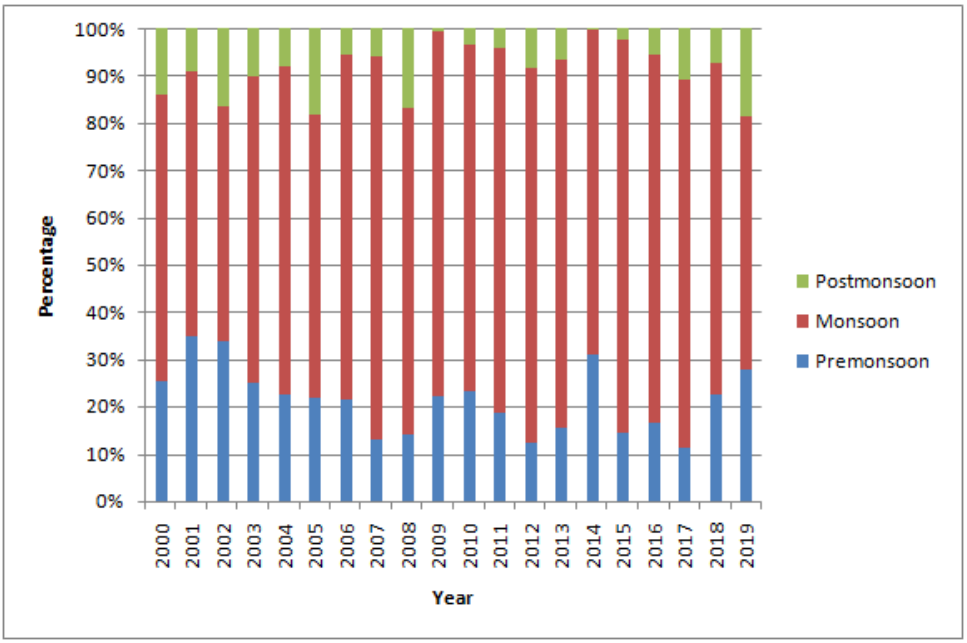

Figure 5.3: Seasonal proportion of yearly rainfall (2000–2019); station: Diamond Harbour.

rate of decrease of the monsoonal rainfall is lower than the pre-monsoon rainfall and the post-monsoon rainfall as indicated by the slopes of the trend lines. To investigate the within-season distribution of yearly rainfall and its change over the years, the rainfall values of the three seasons are plotted together in Figure 5.3. It can be also seen that the variation from the trend line of the rainfall is also lowest in the monsoon season. In several times spans in within the 20-year period under consideration, pre-monsoon and the post-monsoon rainfalls were notably lower than the respective trend lines. For example, from 2007 to 2013, the pre-monsoon rainfall was lower than the trend line, and from 2009 to 2012, the post-monsoon rainfall was lower than the trend line.

To depict the seasonal composition of the yearly rainfall and its variation over the years, the proportions of the yearly rainfall across the seasons are presented in Figure 5.3. It can be seen that the pre-monsoon rainfall is almost always substantially higher than the post-monsoon rainfall. Unsurprisingly, the monsoon rainfall is significantly higher than the pre-monsoon and the post-monsoon rainfalls. No strong indication of a temporal change in the seasonal composition of yearly rainfall can be found from Figure 5.3.

Next, the trends of the monthly rainfalls are investigated, and the plots are presented in Figure 5.4. It is found that the slopes of only February and August rainfalls are positive, and that of December rainfall is only marginally positive. The slopes for the rest of the months are negative. This reflects that these nine months are witnessing declining rainfall. Relatively

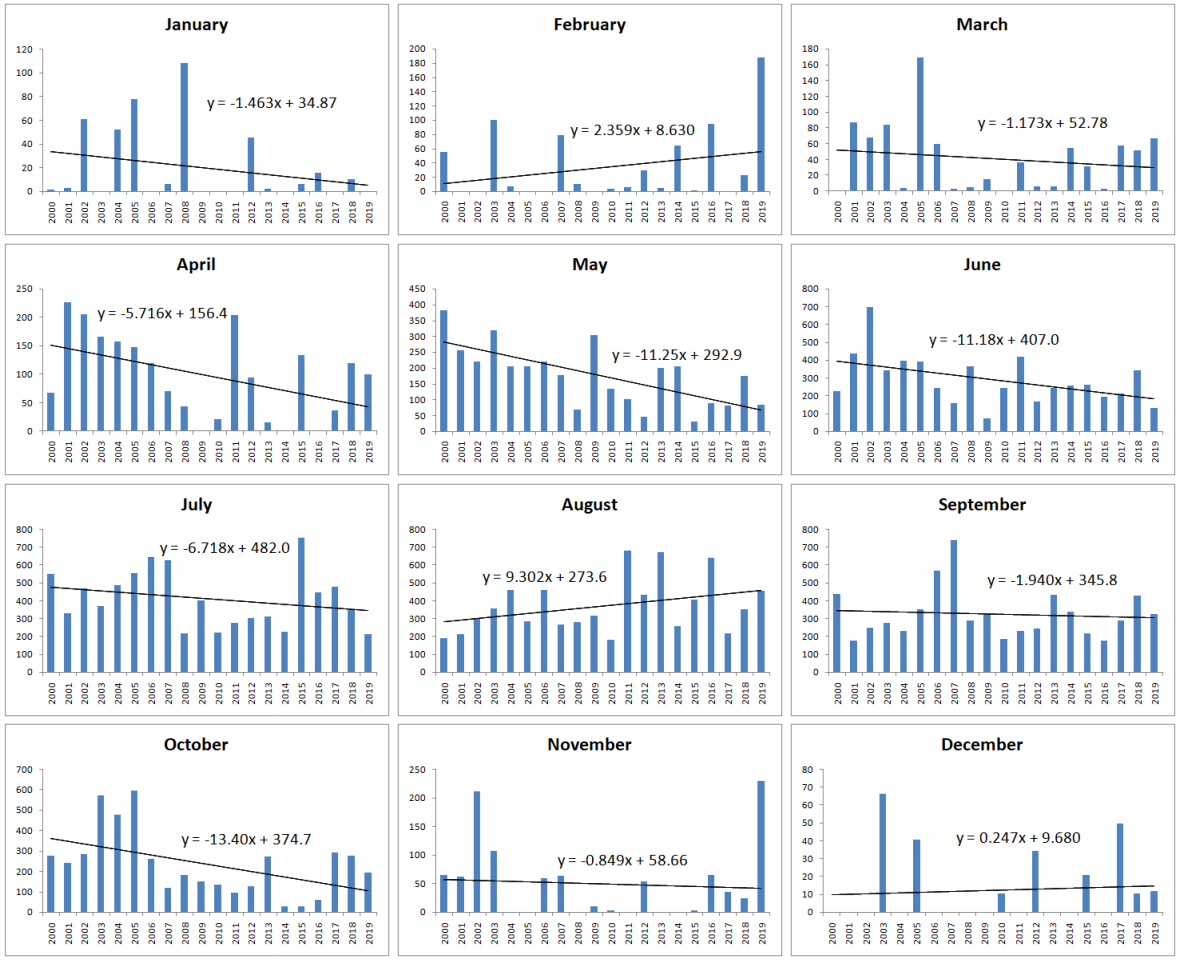

Figure 5.4: Monthly rainfall (2000–2019); station: Diamond Harbour.

sharper decline is the trend is observed for the months of April, May and October. January, March, June and July witnessed moderate decline in rainfall, while September and November witnessed only marginal decline in rainfall.

Overall, from the plots corresponding to yearly rainfall, seasonal rainfall and monthly rainfall, it is clear that there is a decreasing trend in rainfall. The rainfall in all three seasons have decreased. However, the monsoonal rainfall has decreased relatively slowly. Rainfall in most of the months also have decreased, and only three months have exhibited rising trend in rainfall. The decreasing trend of rainfall bears significant implications for the future of the ecology in the south-western Sundarban. As pointed out in an earlier chapter, This region has lack of freshwater influx due to upstream siltation and resulting disconnection of the sources of the local rivers. Decreasing rainfall would further strain the already lacking freshwater budget and hasten salinization. In turn, the mangrove ecology will adversely suffer from such a future scenario. The health of the ecosystem will decline, and the bigger mangrove species will likely

be replaced by more salt-tolerant species.

5.2 Temperature variation

In this section, the temporal variations of the daily maximum temperature and the daily minimum temperature are analyzed over the aforementioned 20-year time period from 2000 to 2019.

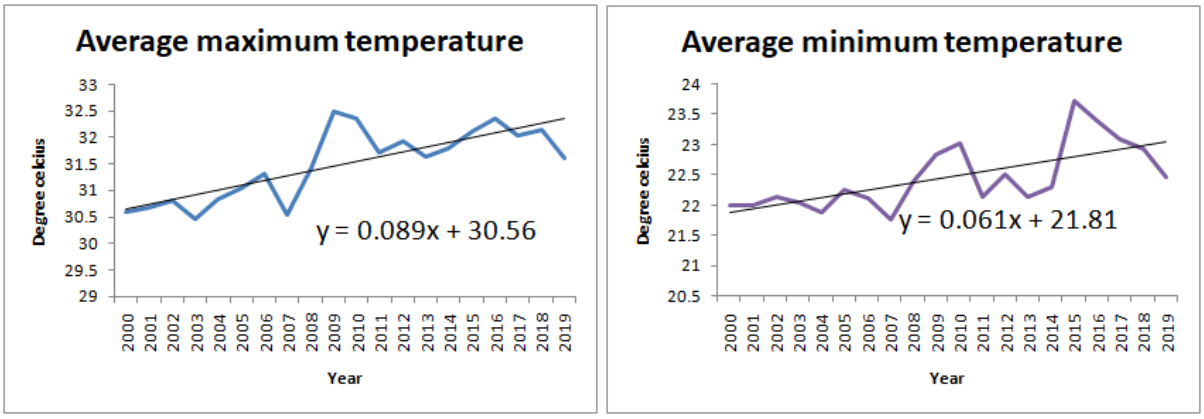

Figure 5.5: Yearly averages of daily maximum temperature and daily minimum temperature (2000–2019); station: Diamond Harbour.

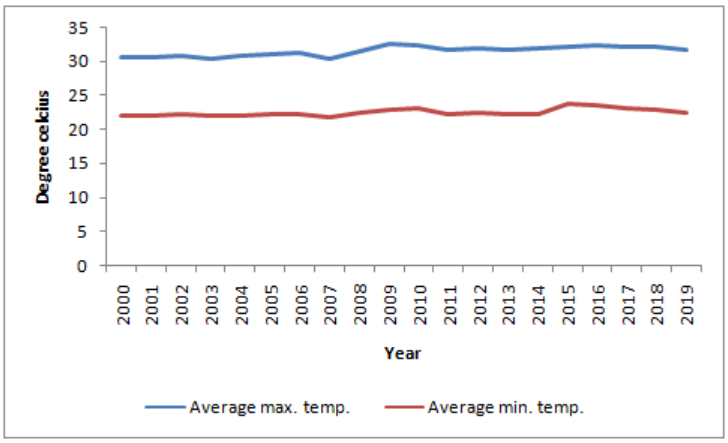

Figure 5.6: Joint plot of yearly averages of daily maximum temperature and daily minimum temperature (2000–2019); station: Diamond Harbour.

To analyze the trend of daily maximum and minimum temperatures, the average daily maximum temperature and the average daily minimum temperatures are computed for each of the 20 years. These yearly averages of the daily maximum and minimum temperatures are presented in Figure 5.5. It is clearly seen that the average daily maximum temperature and the

average daily minimum temperatures have increasing trend. The slope of the linear trend line for the average daily maximum temperature is higher than that of the minimum temperature. This indicates that the daily maximum temperature is increasing in a faster rate than the daily minimum temperature.

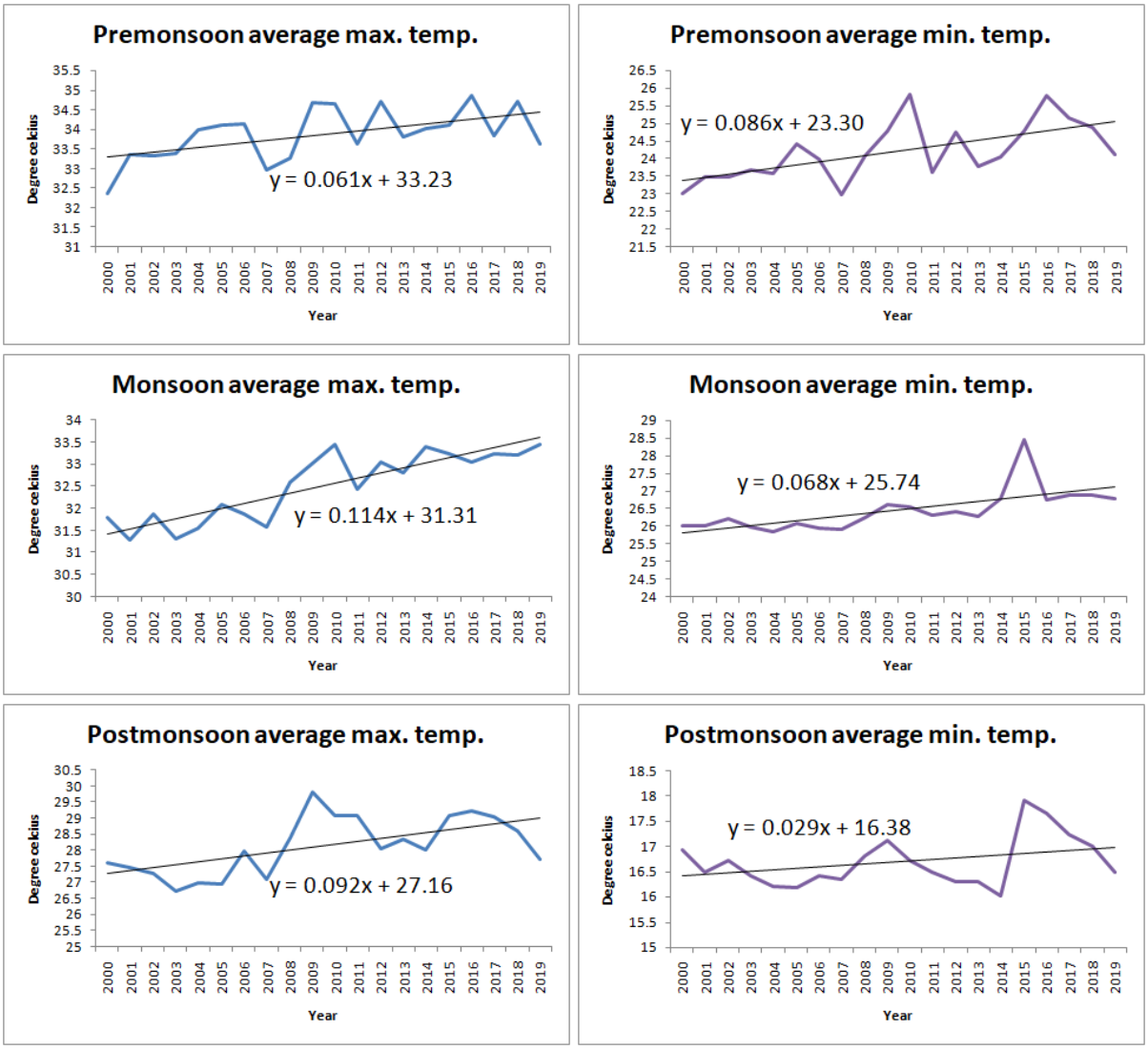

Figure 5.7: Seasonal averages of daily maximum temperature and daily minimum temperature (2000–2019); station: Diamond Harbour.

After observing that both the daily maximum temperature and the daily minimum temperature are increasing, and that the rate of increase of the maximum temperature is higher than that of the minimum temperature, one may be interested in observing whether there is a discernible increase in the gap between the daily maximum temperature and the daily minimum temperature. So, the lines of the daily maximum temperature and the daily minimum temperature are presented in Figure 5.6. The two lines, however, do not exhibit clear signs of diverging

from each other. The gap between them remains almost constant over the time period under consideration.

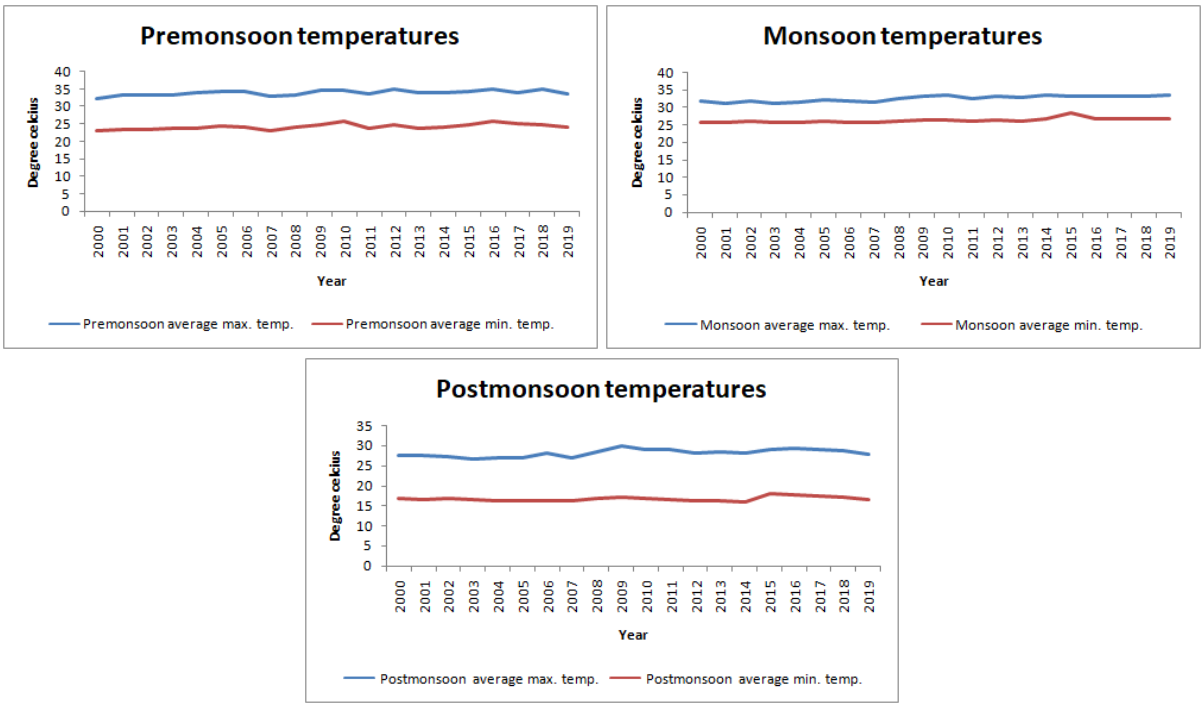

Figure 5.8: Joint plots of seasonal averages of daily maximum temperature and daily minimum temperature (2000–2019); station: Diamond Harbour.

Next, the seasonal trends of the daily maximum and minimum temperatures are investigated. For this, the daily maximum temperatures in a season is averaged for each of the years. Similar averaging is carried out for the daily minimum temperature. The average daily maximum and minimum temperatures are presented in Figure 5.7 for each of the three seasons. In can be seen that every seasonal average of both daily maximum and minimum temperatures exhibit increasing trend. For the daily maximum temperatures, the rate of increase is highest in monsoon. On the other hand, daily minimum temperature increases in the fastest rate in pre-monsoon.

Next, due to the different rates of increase for daily maximum and minimum temperatures, the seasonal average daily maximum and minimum temperature curves are presented for each of the seasons in Figure 5.8 to facilitate a visual comparison of the gaps between daily maximum and minimum temperatures.It can be seen that the gap between daily maximum and minimum temperatures is minimum in monsoon and maximum in post-monsoon. The gap remains more or less constant over the years, which indicates that the different rates of increase of the maximum and minimum temperatures have not yet resulted in a clearly discernible divergence between

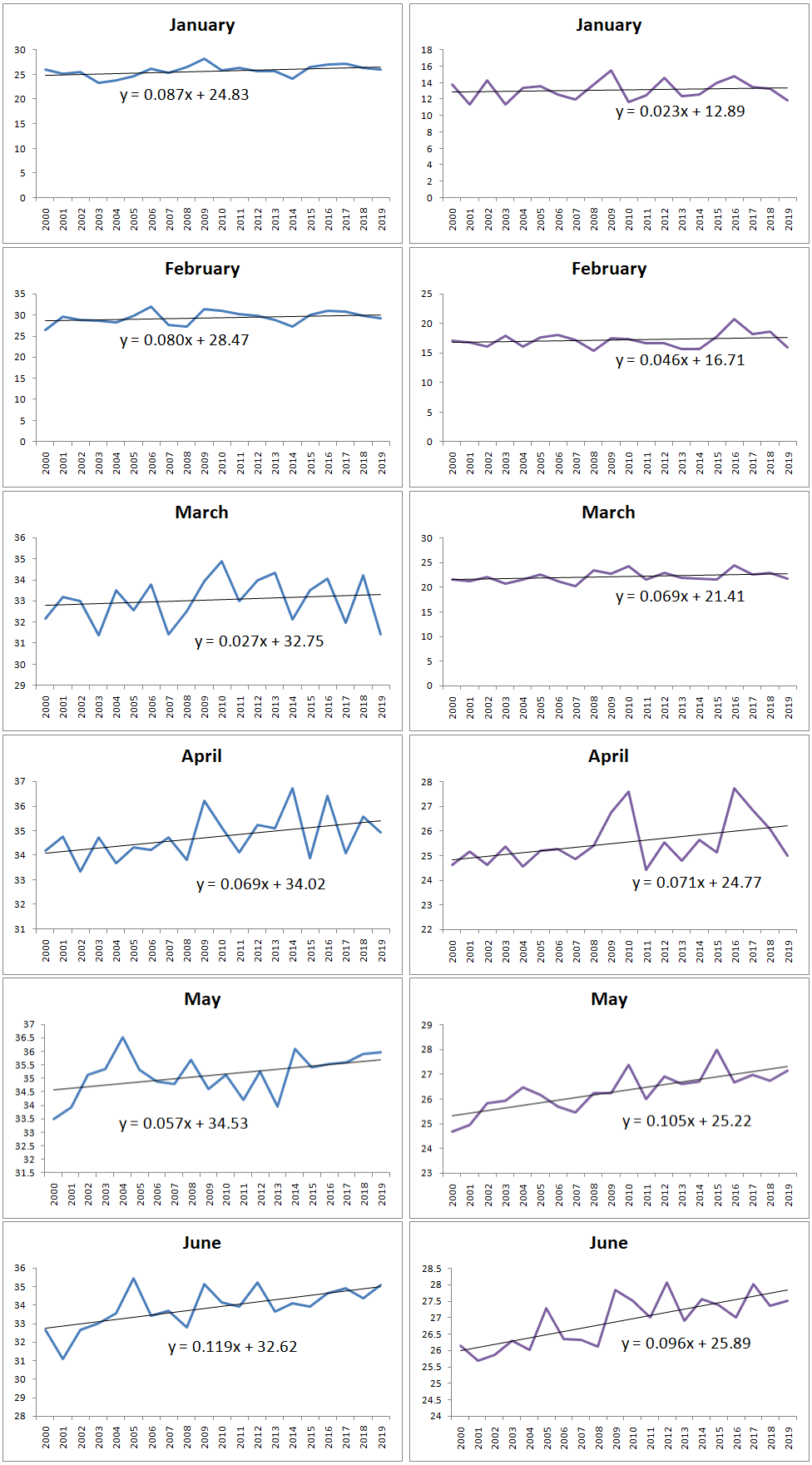

Figure 5.9: Monthly averages of daily maximum temperature and daily minimum temperature from January to June (2000–2019); station: Diamond Harbour.

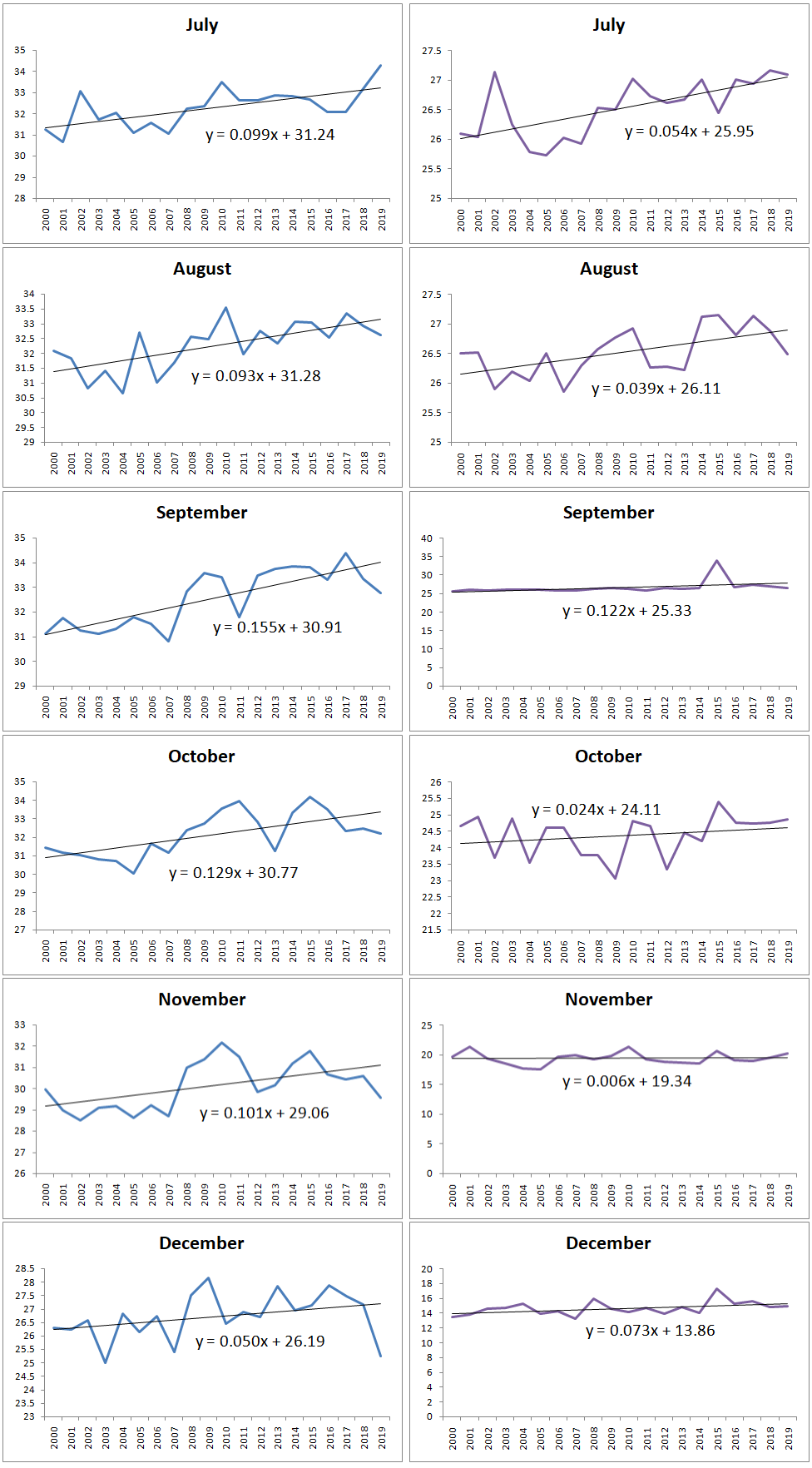

Figure 5.10: Monthly averages of daily maximum temperature and daily minimum temperature from July to December (2000–2019); station: Diamond Harbour.

daily maximum and minimum temperatures.

Subsequently, the trends of the daily maximum and minimum temperatures are analyzed for each of the months separately. For this, the daily maximum temperature is averaged within each month for each of the years and similar averaging is carried out for the daily minimum temperature. The monthly averages of the daily maximum and minimum temperatures are presented in Figure 5.9 for the months from January to June and in Figure 5.10 for the months from July to December. It is observed that average daily maximum and minimum temperatures exhibit positive trends for every month. The positive trends for the daily maximum temperature are especially strong in the monsoon months and the post-monsoon months of November and December. This along with the previous observation on the trend of the average daily maximum temperature indicates that the daily maximum temperature has risen fastest in the monsoon times. The trends for the average daily minimum temperature are the stronger in the pre-monsoon months and September. This indicating that the daily minimum temperature has risen fastest predominantly in the summer months.

5.3 Changes in relative humidity

To investigate the trend of relative humidity over time, two series of daily relative humidity measurements are used. One of them, denoted as relative humidity (I), is measured daily in the morning, and the other, denoted as relative humidity (II), is measured daily in the evening. The

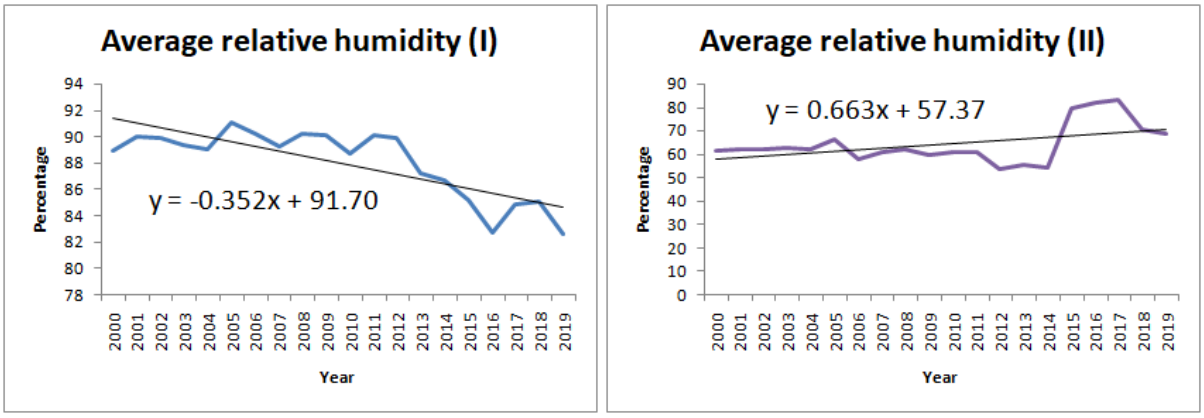

Figure 5.11: Yearly averages of daily relative humidity measurements (2000–2019); station: Diamond Harbour.

reason behind considering the two relative humidity measurements is that the drop in temperature in the night causes a rise in the relative humidity, and similarly the higher temperature during

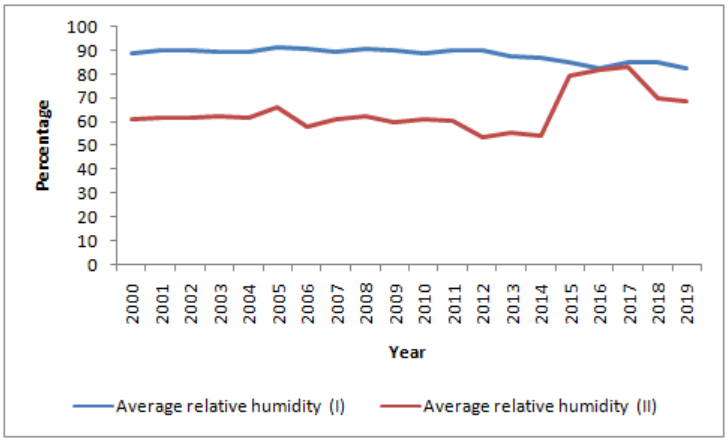

Figure 5.12: Joint plot of yearly averages of daily relative humidity measurements (2000–2019); station: Diamond Harbour.

the day caused a fall in relative humidity if other conditions remain fixed. Like in the case of daily maximum and minimum temperatures considered in the previous section, the yearly averages of the two relative humidity measurements are presented in Figure 5.11.

It can be seen that one of the measurements, relative humidity (I), which is recorded in the morning, exhibits clear decreasing trend. The other one, relative humidity (II), exhibits upward trend. However, on closer inspection, it can be seen that the relative humidity values for the second measurement, i.e., relative humidity (II), behave differently after 2015. If trend analysis is done by dropping the values after 2015 in the case of relative humidity (II), then it would have a decreasing trend. To visually inspect the gao between relative humidity (I) and (II), the lines are plotted together in Figure 5.12. It can seen that the relative humidity (II) series abruptly jumps at 2015 to touch relative humidity (I), and start to diverge only at 2018 onward. Except this, the two series show visual indication of a slight divergence before 2015.

In Figure 5.13, the seasonal averages of the daily relative humidity measurements are presented. There, one can observe that the relative humidity (I) series exhibits declining trend in all the seasons. The declining trend in the pre-monsoon season and the post-monsoon season are stronger than that of the monsoon season. However, there is a jump in the average daily relative humidity (I) in the monsoon in the year of 2017. This abrupt jump may have affected the trend line. The relative humidity (II) series shows positive trends in the seasons. However, they also clearly show a sudden jump at 2015. This jump is conspicuous for the pre-monsoon season and the post-monsoon season. For the monsoon season, the jump is more subdued, but presents like a phase shift. If trend analysis is carried out before this jump, then the relative

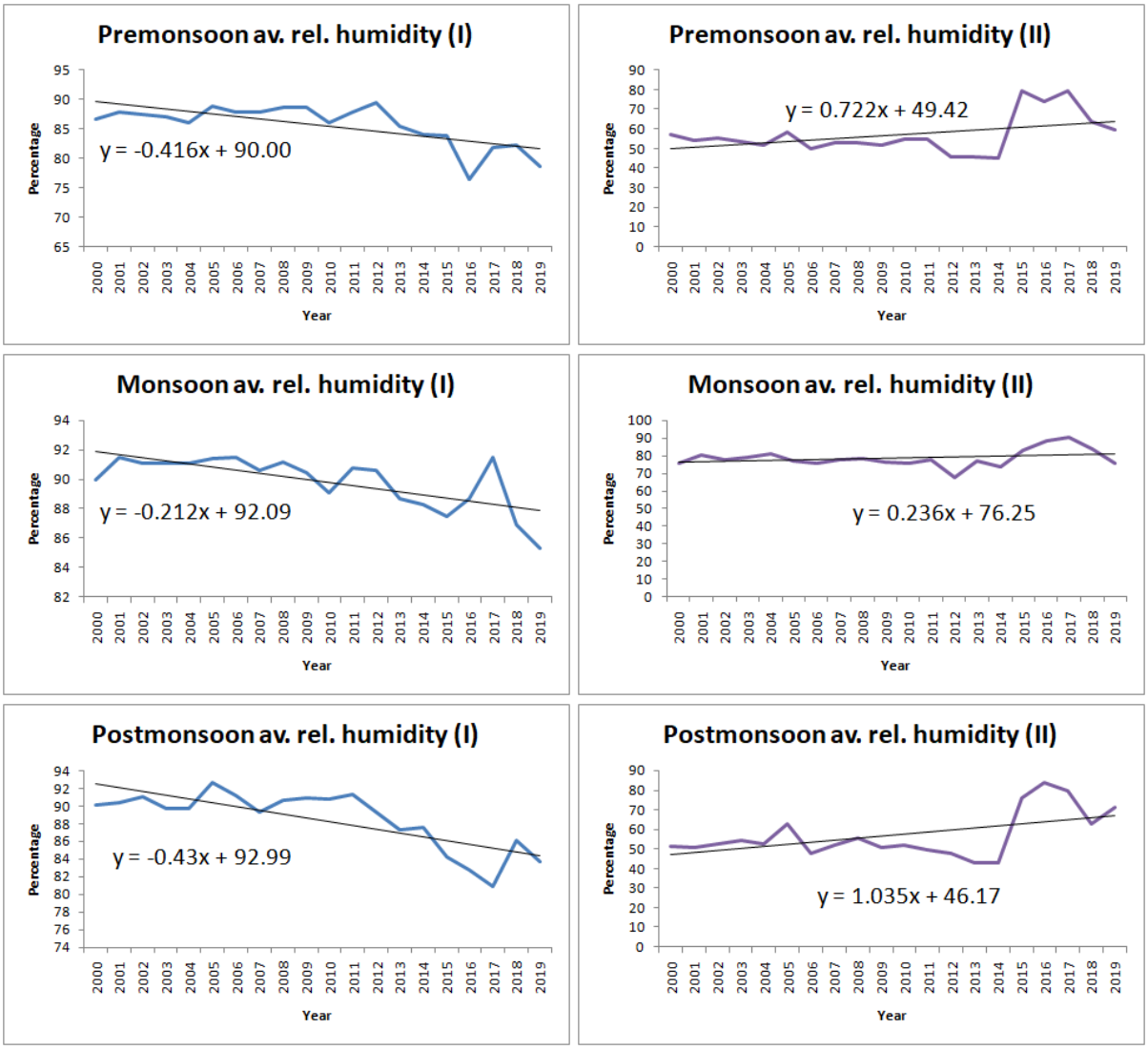

Figure 5.13: Seasonal averages of daily relative humidity measurements (2000–2019); station: Diamond Harbour.

humidity (II) series also exhibits decreasing trend. It is notable that after the change in 2015, the relative humidity (II) series again starts to decrease across the seasons at 2017.

Next, to visually examine the gap between the two series of measurements, the seasonal averages of relative humidity (I) and relative humidity (II) are presented together in Figure 5.14. Here, except the abrupt change in the relative humidity (II) series at 2015, the two series exhibits a slight hint of divergence before 2015 across the seasons. The abrupt change in the relative humidity (II) series makes the two series almost coincide for the years 2015 to 2017. However, after that, the two series separate and show signs of divergence again.

Subsequently, the monthly trends of the relative humidity measurements are analyzed by averaging each of the relative humidity series within a month and then plotting the averages for

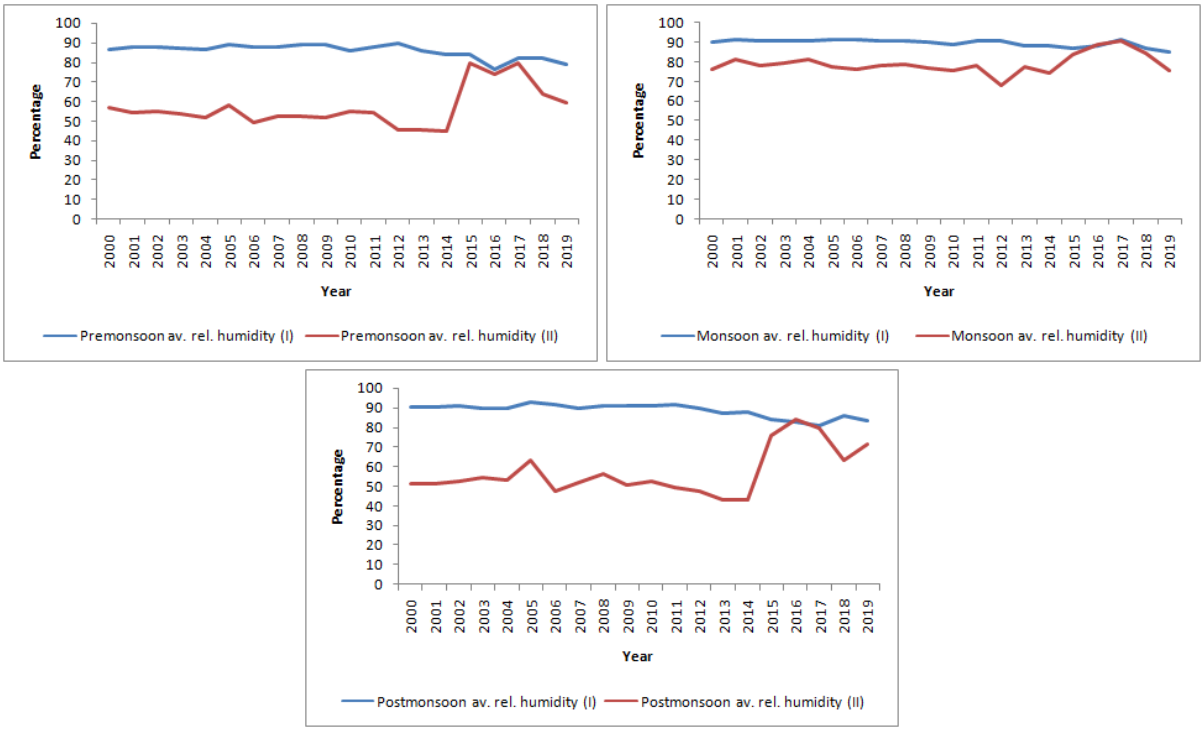

Figure 5.14: Joint plots of seasonal averages of daily relative humidity measurements (2000–2019); station: Diamond Harbour.

that month over the years. The monthly averages of the relative humidity measurements are presented in Figure 5.15 for the months from January to June, and in Figure 5.16 from July to December.

5.4 Evapotranspiration rate

The potential evapotranspiration (PET) is calculated using the Thronthwaite method (Thornthwaite, 1948). Using this method, the monthly potential evapotranspiration rate is first estimated for every month in the 20-year period under consideration. After this estimation, the yearly potential evapotranspiration is computed by summing the monthly potential evapotranspiration for each of the months in that year. The yearly potential evapotranspiration is presented in Figure 5.17. It exhibits a clear increasing trend. [h]

Observing the increasing trend of potential evapotranspiration, one may be interested in examining whether the yearly rainfall may sustain the potential evapotranspiration. To examine this, the joint plots of the yearly rainfall and the yearly potential evapotranspiration are presented in Figure 5.18. One can observe that the yearly potential evapotranspiration rate exceeded the

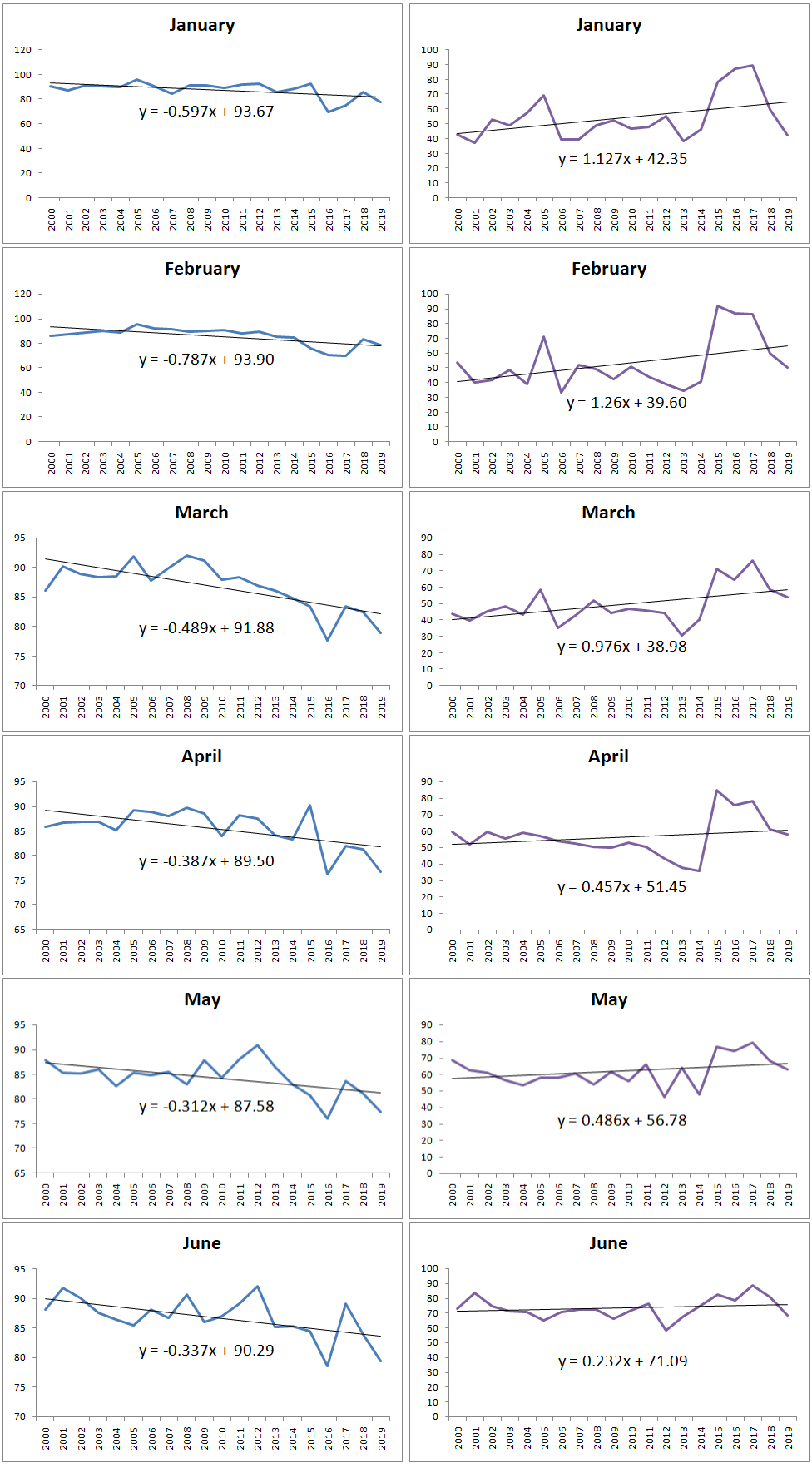

Figure 5.15: Monthly averages of daily relative humidity measurements from January to June (2000–2019); station: Diamond Harbour.

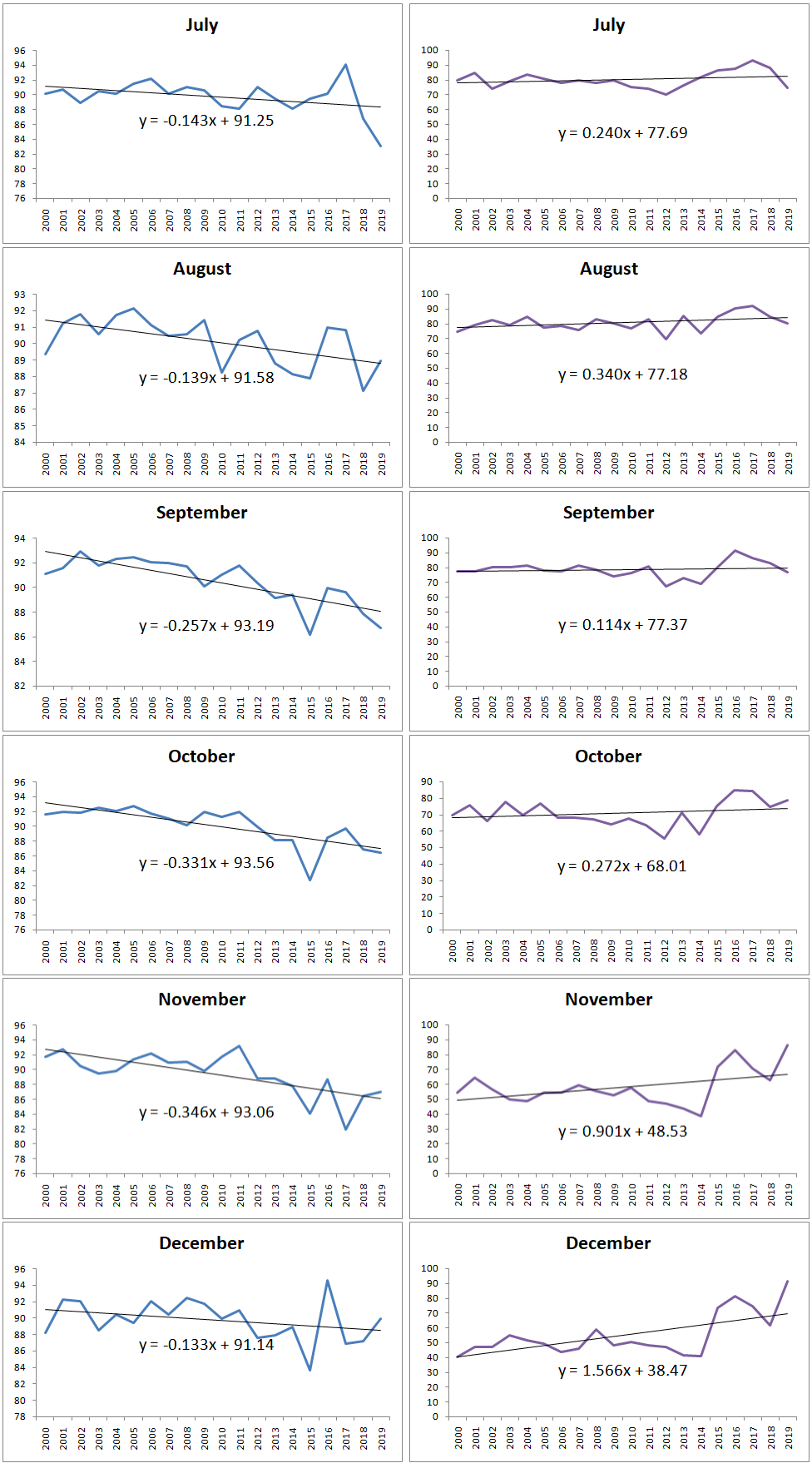

Figure 5.16: Monthly averages of daily relative humidity measurements from July to December (2000–2019); station: Diamond Harbour.

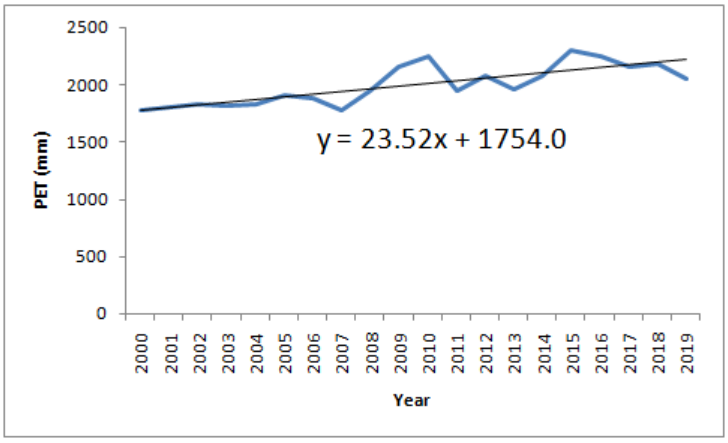

Figure 5.17: Yearly potential evapotranspiration (2000–2019).

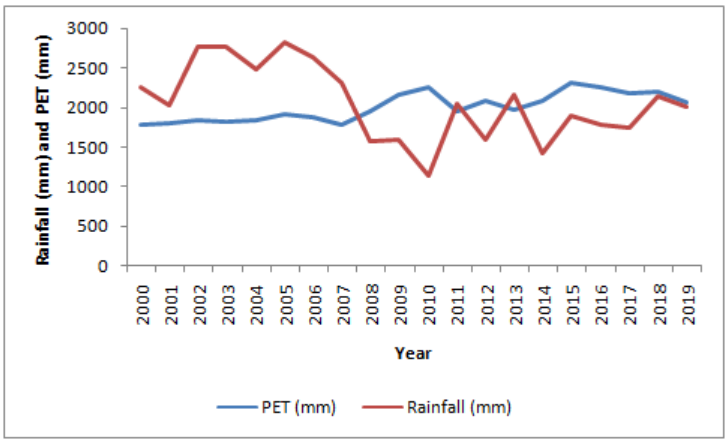

Figure 5.18: Comparison of yearly potential evapotranspiration and rainfall (2000–2019).

yearly rainfall in 2008 and almost always is higher than the yearly rainfall afterwards. Only in 2011 and 2013, the yearly rainfall narrowly exceeds the yearly potential evapotranspiration, only to again fall back. However, in 2018 and 2019, the yearly rainfall is very close to the yearly potential evapotranspiration, though still smaller than the later.

Noticing the upward trend of the yearly potential evapotranspiration, one may be interested in examining the trends of the monthly potential evapotranspiration. So, the monthly potential evapotranspiration rates are presented in Figure 5.19. There, the potential evapotranspiration in each of the months exhibit increasing trend. The trend is stronger in the monsoon months and the late pre-monsoon months of April and May. The post-monsoon months of November, December and January exhibit a weaker increasing trend. This indicates that the potential evapotranspiration has increased in the monsoon months and the pre-monsoon months before the onset of the monsoon, due to the increasing temperature in that period.

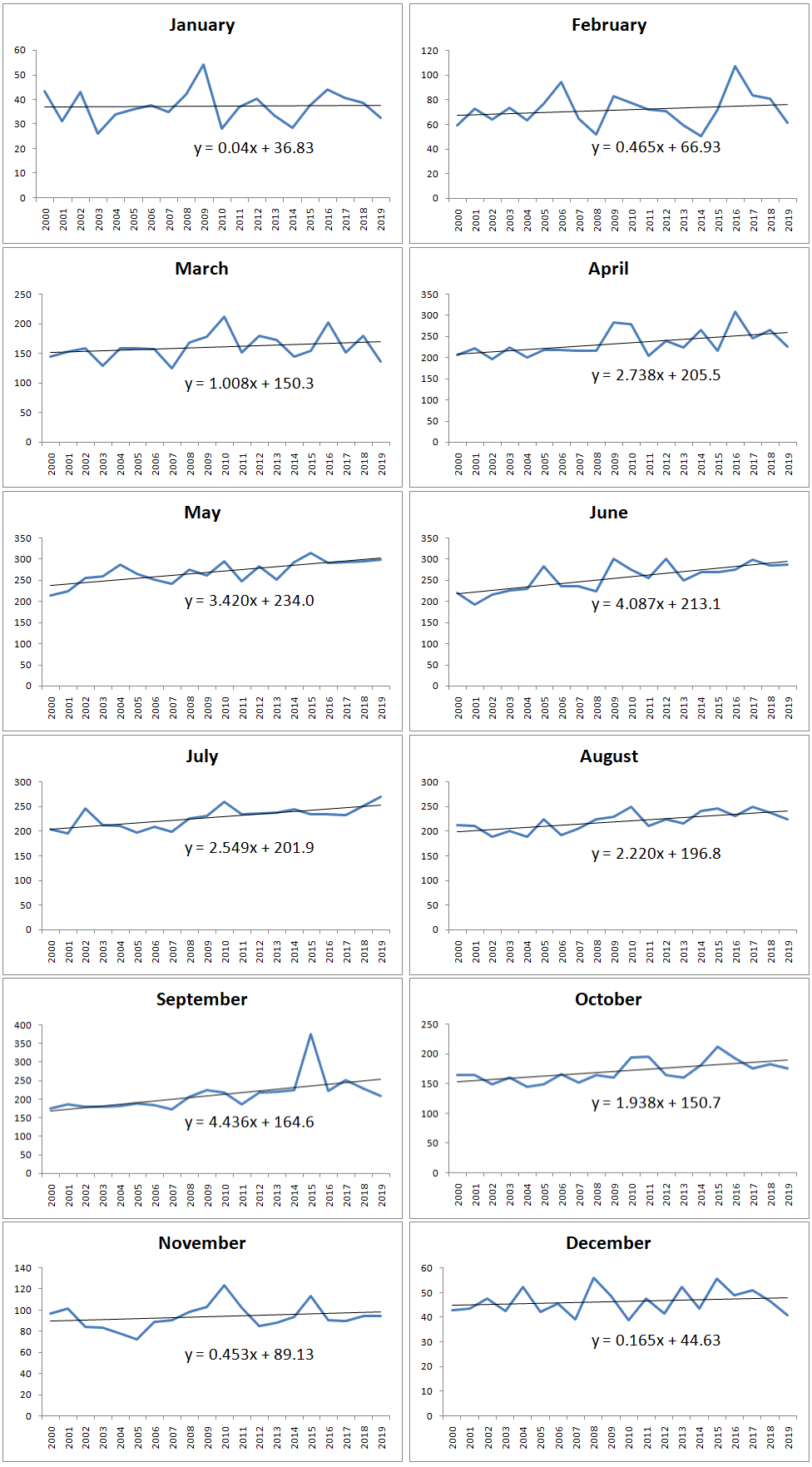

Figure 5.19: Monthly potential evapotranspiration (2000–2019).

5.5 Mangrove forest cover areas of the islands with classes

The forest cover in the islands in the islands differ in character, primarily because of anthropogenic influence. Because the Henry's island is a center of significant human activities, a large portion of the natural forest in this island is cleared. Some artificial plantation of mangroves and other trees is also carried out by the government and the local community to guard against soil erosion and storm devastation. On the other hand, the Patibania island, being mostly protected from human influence, witnesses its forest growing under the influence of natural processes only. Among the natural processes, the influence of tidal inundation is paramount. The intertidal zones and the supratidal zones exhibit significant divergence in the plant species growing there. The mangrove zonation in both the islands are examined using field visits and satellite imagery, and it was found that tidal inundation level and topographic features mostly determine the mangrove characteristics in a region.

The density of vegetation in the islands is found to vary spatially and temporally. In Figure 5.20, the vegetation index maps of the two islands are presented for the years 2009 and 2016. The density of vegetation in both the islands is divided into four classes: high, medium, low and very low. It can be observed that the vegetation density in the two islands differ in their spatial distribution and also temporal variation. The overall density of vegetation in the Henry's island is found to decrease in 2016 compared to 2009, while that of the Patibania island is found to slightly increase in 2016. The most significant decrease in the density of vegetation in the Henry's island has occurred in the northern and the north-eastern parts, while in some small areas in the south-western part of the island, the vegetation density is found to increase marginally. In the Patibania island, the vegetation density is found to increase in the northern part and the south-western part. However, in some pockets in the north-central part and the western coast of the middle south part of the island, the vegetation density is found to marginally decrease. In the Henry's island, the densest vegetation is found in the south-western part and around the aquacultural ponds. In the Patibania island, the densest vegetation is observed on the eastern side of the island.

The vegetation index however only reflects the density of vegetation, and cannot depict the mangrove zonation characteristics. Field visits are necessary to examine and identify the mangrove zonation. Based on the field observations, it is found that tidal inundation and water influx through the creeks play salient roles in determining mangrove zonation in the islands.

In the littoral zone in the Henry's island, the herbaceous plants cannot form dense vegeta-

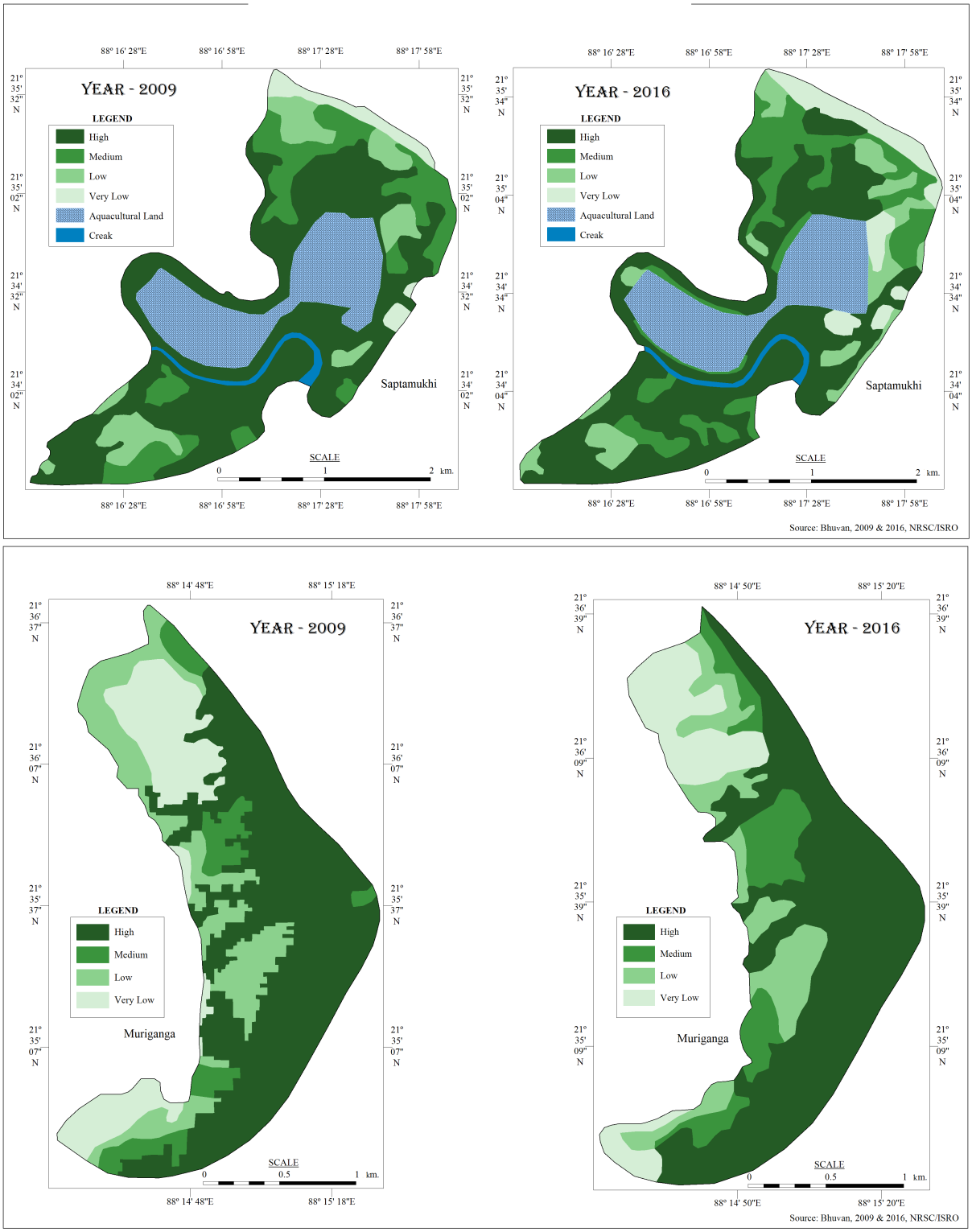

Figure 5.20: Change in vegetation index in the two islands.

tion. But, in the elevated parts of this zone which seldom undergoes inundation, the artificial plantation contains woody plants that are able to grow dense foliage and form canopy cover. So, the density of vegetation is very high in this mangrove forested area that is created artificially. In the tidal flats in portions of the seashore, vegetation density also varies based on which part of the tidal flat is under consideration, the upper tidal flat, the middle tidal flat or the lower tidal flat. In the lower tidal flat, due to the unconsolidated nature of the soil and wave action, little foliage can grow. However, the quantity of foliage increases as one proceeds towards the upper tidal flat. In the inland areas behind the littoral zone under the influence of tidal drainage loss and resultant increase in salinity in the soil, the growth of mangrove hampers, and the density of vegetation is low. In the saltpans formed in this region, vegetation is either nonexistent or sparse. However, further inland where the creeks transport water, patches of true mangrove forests have developed with canopy cover and dense foliage. Vegetation is also naturally very dense here.

The eastern coast of the Patibania island has the highest density of vegetation. This high density is a result of the copious tidal water influx from the Edward's creek. The diverse mangrove species growing there contains woody true mangrove trees with lush foliage and well-formed canopy cover. However, next inland from this zone, the stunted mangroves resulting from relatively scant water available cannot generate much leaf growth. Hence, vegetation density is relatively low here. In further inland, in the salt marsh zone, the higher salinity level hinders the growth of mangroves, and results in low density of vegetation. However, salinity further increases inland, resulting in saltpan formations. The very high salinity in the saltpans prevents proliferation of almost all mangrove species, resulting in a landscape that is almost barren. Vegetation is thus sparse here. Further to the west, one reaches the western boundary of the Patibania island. Here in the littoral zone, most plant life is herbaceous in nature. Though this plants proliferate well, they cannot sustain lush foliage due to continuous wave and tidal action. So, vegetation density is moderate here. However, near the western seashore where the elevation in relatively higher, the abundant water availability creates favorable conditions for the growth of patches true mangrove forests, which has a high density of vegetation.

In Plate 5.1, photos of the vegetation species and the topography in the different vegetation zones in the Henry's island are presented. Photos of the species and the landscape of the vegetation zones in the Patibania island are presented in Plate 5.2.

Plate 5.1: Mangrove zones with different vegetation densities in the Henry's island: within saltpan (first row, left), fringe area (first row, right), moderately dense mangroves (second row, left), vegetation in a premature saltpan (second row, right), mangroves of low density (third row, left), dense mangroves (third row, right), salt marshes along the shoreline (fourth row, left), salt marsh vegetation at low tidal flats (fourth row, right).

Plate 5.2: Mangrove zones with different vegetation densities in the Patibania island: dwarf mangroves in a saltpan (first row, left), moderately dense mangroves in the fringe area of a saltpan (first row, right), degraded vegetation (second row, left), dense vegetation (second row, right), vegetation of low density on an overwash deposit (third row, left), mangrove plantation along the tidal shore bar (third row, right).

5.6 Relationship of mangrove forest cover area with climate

Mangroves are in general robust and adaptable to changes in environment up to a degree. However, changes in environmental conditions leave their marks on the characteristics of the mangrove ecology. The ongoing climate change is a cause of concern regarding the health of the mangrove ecology. It is demonstrated earlier in this chapter that in the south-western Sundarban region, rainfall is declining (Section 5.1) and temperature is rising (Section 5.2). Here, the relationship of the mangrove forest cover with the climate variables are investigated.

In the Patibania island, due to it being a reserve forest, the mangroves grow an proliferate naturally with minimal or negligible human interference. So, this island is an ideal place to investigate the effect of climate on the natural growth of mangroves. In the Henry's island however, human activities have significant impact on the mangroves, both positive and negative. Substantial areas are cleared of mangroves for economic enterprises, while extensive plantation of mangroves are developed by the forest department and the local community to weather impacts of erosion and storm damage. So, analysing the relationship of mangrove forest cover and the climate variables in the Henry's island may not provide an unbiased picture of the dependence of mangroves on the climate. In this section, the effect of climate on the mangrove forest cover in the Patibania island is studied first. Then, as an academic curiosity, the same analysis is carried out for the Henry's island, though keeping in mind that the results in the case of the Henry's island may not present the effect of climate on natural mangrove growth.

For the analysis, the areas covered by dense mangroves, mangroves of moderate density, mangroves of low density and mangroves of very low density in the years 2005, 2010, 2015 and 2019 are considered in each of the islands. So, there are four variables corresponding to mangrove forest cover, which correspond to dense mangroves and mangroves of moderate, low and very low densities, and each variable has four observations corresponding to the four years 2005, 2010, 2015 and 2019. For these four years, the yearly total rainfall, the yearly average of daily maximum temperature, the yearly average of daily minimum temperature and the yearly averages of daily relative humidity (I) and (II) values respectively are considered as covariates. For each pair of a variable corresponding to mangrove forest cover and a climate variable, a linear regression is carried out taking the forest cover variable as response and the climate variable as the covariate. For each regression, the R^2 value is computed to measure the strength of the regression.

For the Patibania island, the regression lines along with the corresponding R^2 values are

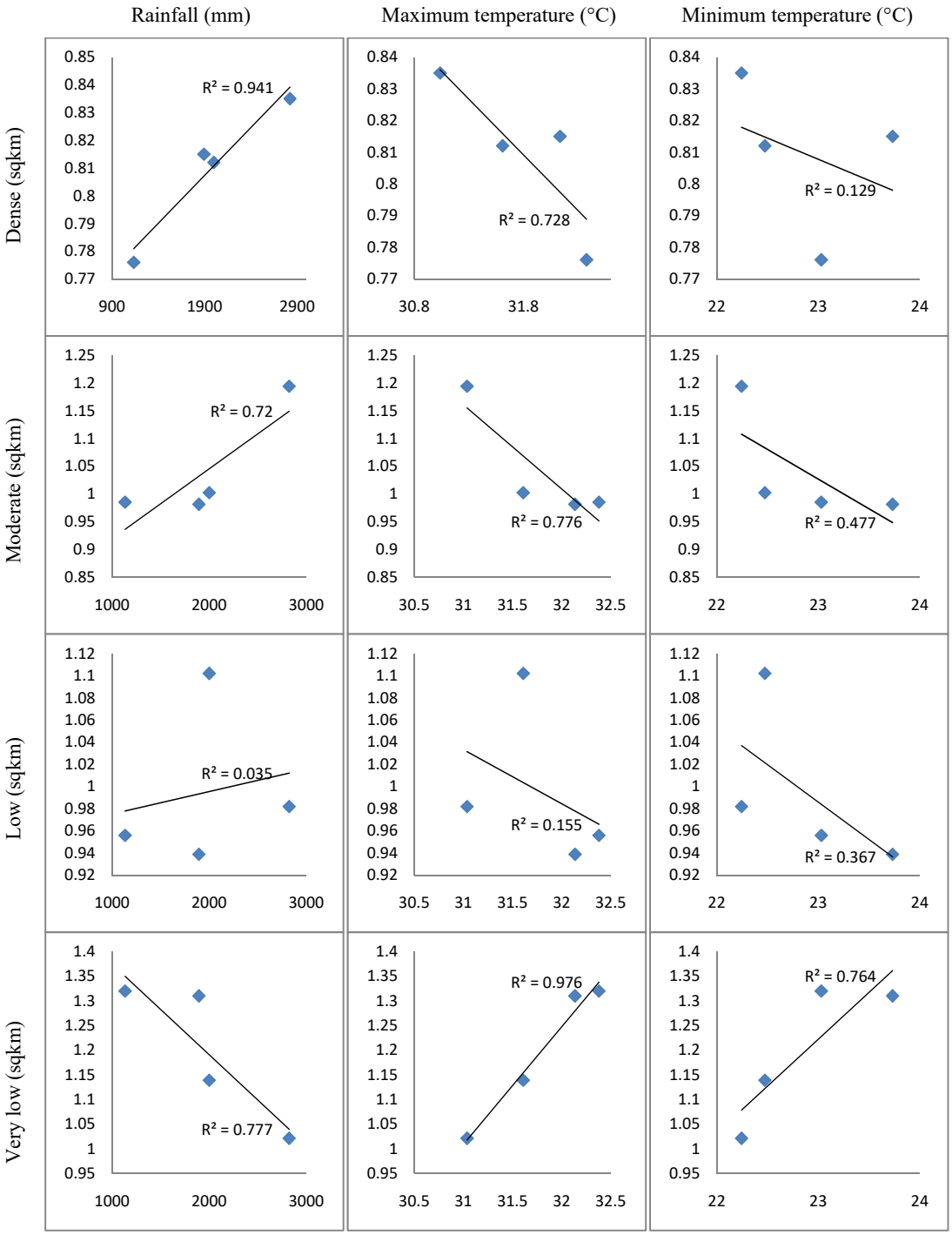

Figure 5.21: Regression of mangrove forest cover of different categories on yearly rainfall, average daily maximum temperature and average daily minimum temperature in the Patibania island.

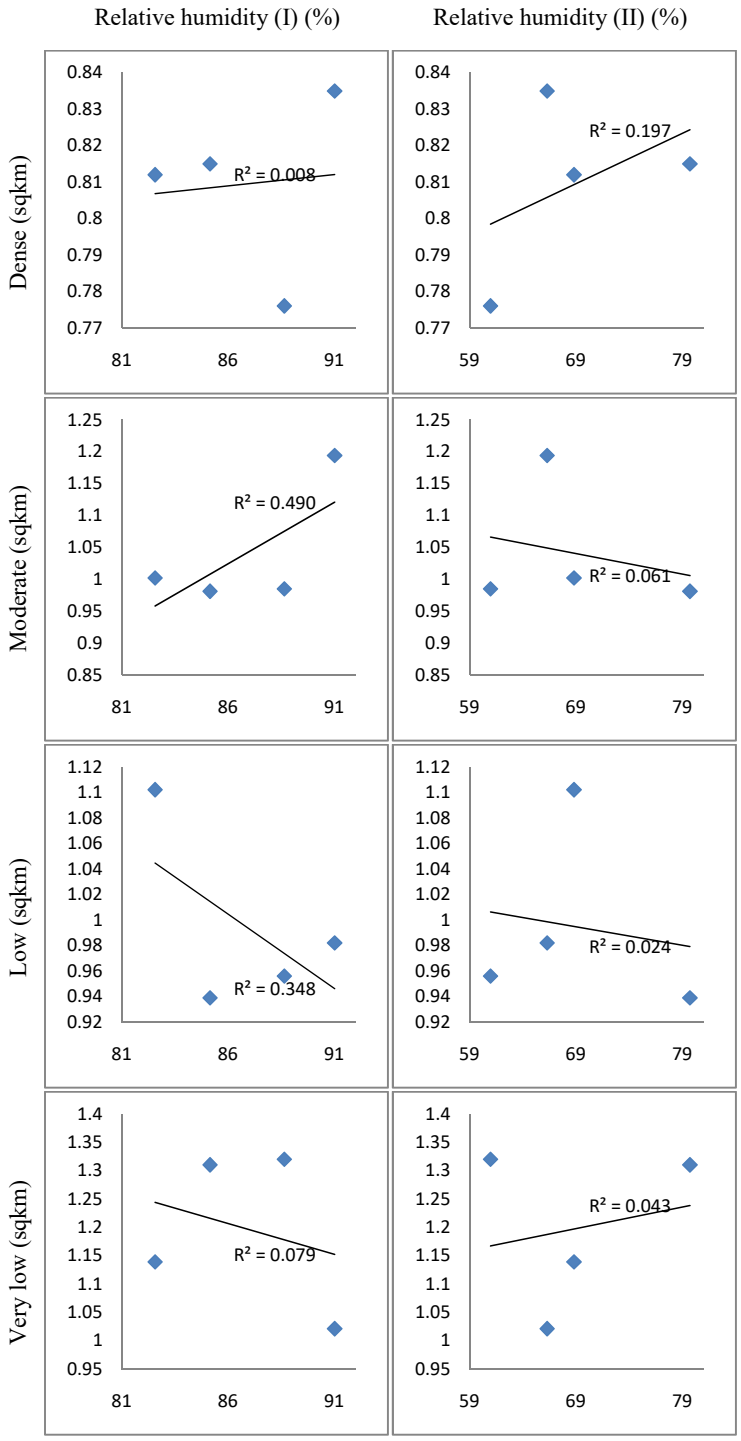

Figure 5.22: Regression of mangrove forest cover of different categories on yearly averages of daily relative humidity values (I) and (II) in the Patibania island.

presented in Figure 5.21 for the covariate being one of the yearly total rainfall, the yearly average of daily maximum temperature and the yearly average of daily minimum temperature, and in Figure 5.22 for the covariate being one of the yearly averages of daily relative humidity (I) and (II) values.

From Figure 5.21, it can be observed that for each of the response variables corresponding to dense mangroves and mangroves of moderate and low densities, the slopes of the regression lines with rainfall as the covariate is positive, and the slope of the regression line of the variables corresponding to mangroves of very low density with rainfall as the covariate is negative. The R^2 value is highest for the response variable corresponding to dense mangroves, and the next highest is for the response variable corresponding to mangroves of very low density. This clearly indicates that an increment of rainfall has positive impacts on dense mangroves and mangroves of moderate and low densities but negative impact on mangroves of very low densities. The slopes of the regression lines suggest that as rainfall increases, significant portions of the areas covered in mangroves of very low densities transform to become covered in mangroves of low densities, on the other hand some areas covered in mangroves of low and moderate densities become covered in mangroves of moderate density and dense mangroves, respectively. The very high R^2 value for the regression involving the area covered in dense mangroves and rainfall indicates the very strong relationship between them. On the flip side, the same results point out that as rainfall declines, areas covered in dense mangroves are badly affected, mangrove density decreases overall and areas under mangroves of very low density increases.

From the slopes of the regression lines in Figure 5.21 when the covariate is one of maximum and minimum temperatures, it can be seen that as temperature increases, areas under dense mangroves and mangroves of moderate, low and very low densities decrease, only the area covered by mangroves of very low density increases. The R^2 values indicate that the relationship between temperature and areas under dense mangroves and mangroves of moderate and very low densities are very strong. All, these indicate that with rising temperature, mangroves are harmed and their density decreases notably.

The relationship between mangrove density and relative humidity, as reflected from the R^2 values of the regressions in Figure 5.22, are not as strong and as clear to interpret. However, it can be observed that with rise in relative humidity, the area under dense mangroves increases.

The regression lines along with the R^2 values for the Henry's island are presented in Figure 5.23 and Figure 5.24. Surprisingly, though the mangroves in the Henry's island are con-

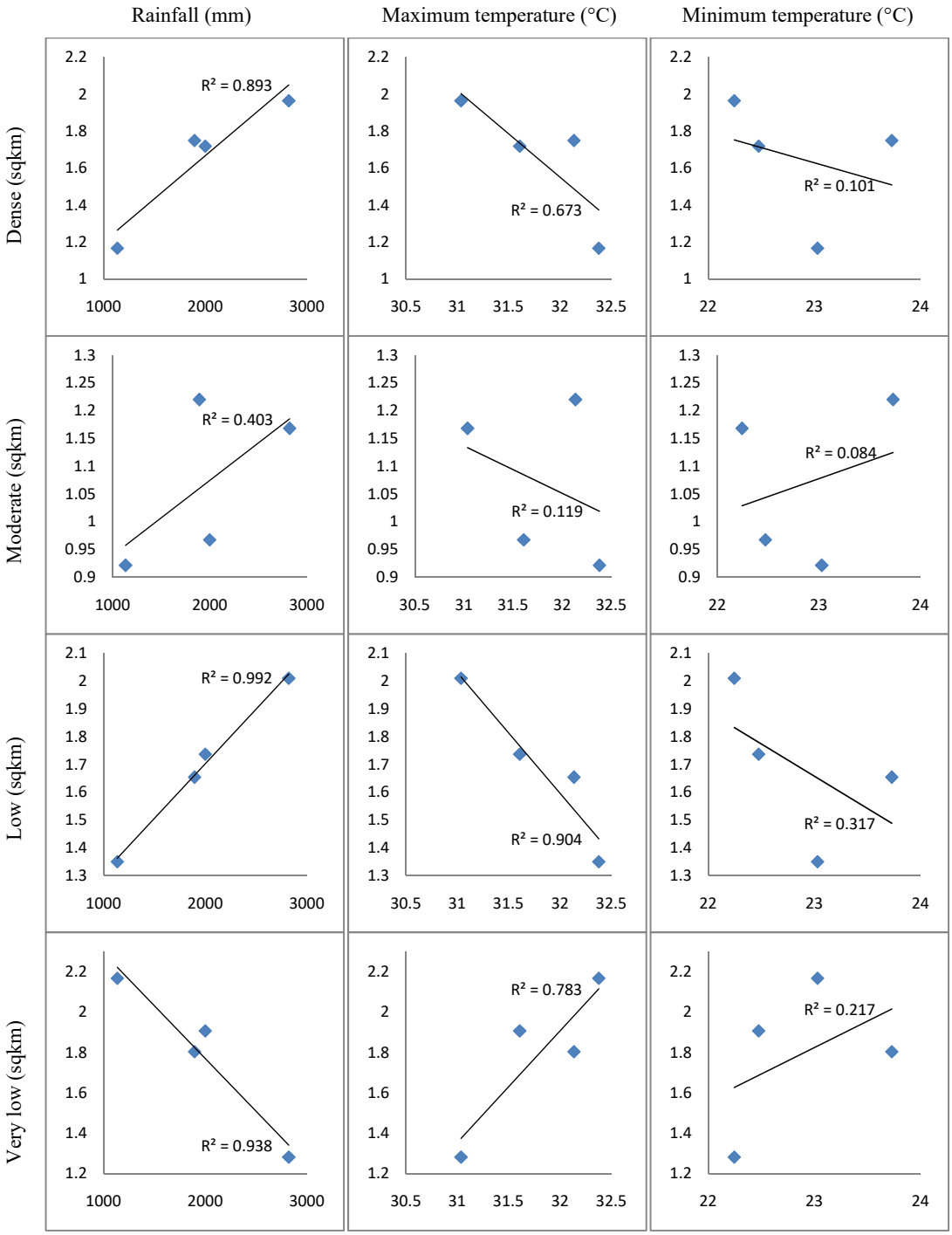

Figure 5.23: Regression of mangrove forest cover of different categories on yearly rainfall, average daily maximum temperature and average daily minimum temperature in the Henry's island.

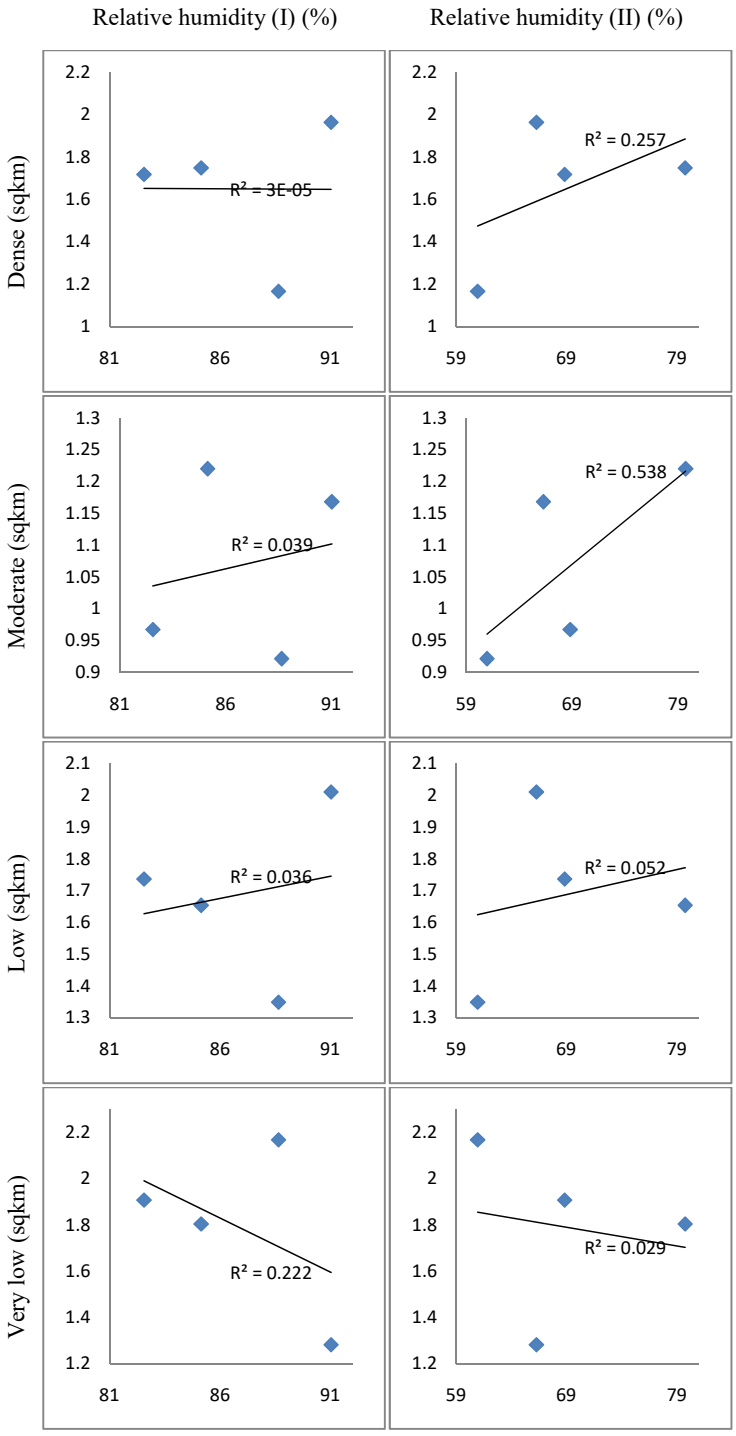

Figure 5.24: Regression of mangrove forest cover of different categories on yearly averages of daily relative humidity values (I) and (II) in the Henry's island.

siderably affected by human activity, the same patterns for the relationships between mangrove density and rainfall, maximum and minimum temperatures prevail. The relationship between mangrove density and relative humidity is again not so strong or clear.

The above findings about the relationship between mangrove density and climate variables have profound implications. It is already seen in Section 5.1 and Section 5.2 that rainfall is declining and temperature is increasing in the south-western Sundarban region. In the above analysis, it is found that with declining rainfall, mangrove density is strongly affected. The same happens with increasing temperature. Also, the relationships are considerably strong. This implies that the ongoing climate change is likely to significantly affect the mangroves in the south-western Sundarban region. The density of the mangroves will decrease, many areas may transform to sparsely vegetated or almost barren wastelands.

5.7 Biomass estimation of mangroves

Mangroves form productive ecosystems and capable of sequestering a large amount of atmospheric carbon (Rahman et al., 2015). The biomass of a plant is its dry weight, a significant part of which is carbon. Due to obvious practical problems in measuring the dry weight of a plant, several allometric methods are developed to estimate the biomass of mangroves (Komiyama et al., 2008). In Machiwa and Hallberg (2002), the organic carbon dynamics of a mangrove ecosystem is investigated. In Komiyama et al. (2005), several allometric equations were studied for the estimation of the weights of several parts of a mangrove tree including its trunk, aboveground part, root and also leaves. In (Komiyama et al., 2000), Khan et al. (2007) and Jones et al. (2014), biomass and carbon stock in some mangrove species and in different ecologies were estimated and studied. The salinity level also influences the biomass of the mangrove species, with higher salinity levels facilitating biomass accumulation of some species and hindering others (Banerjee et al., 2013). It was observed by Kamruzzaman et al. (2017) that the biomass of mangroves in regions with less salinity levels, where larger mangrove trees like *Heritiera fomes* propagate well (Rahman and Islam, 2015), is higher than regions with higher salinity levels. In fact, it was found by Rahman et al. (2015) that forests dominated by *Heritiera fomes* contained the highest amount of ecosystem carbon per unit area in Sundarban.

Forests in the northern hemisphere serve a paramount role as a carbon sink (Goodale et al., 2002), and mangrove forests are among the most carbon-rich in the tropics, containing a very

significant portion of the carbon stock despite occupying relative minute portion of the forest area (Donato et al., 2011). The estimation of biomass of mangroves in the south-western Sundarban, a significant mangrove habitat, is thus an important endeavor due to the remarkable role of the mangroves in carbon sequestration.

In the Henry's island, the biomass estimation was carried out in three years, 2006, 2009 and 2019. Both above ground and below ground biomass were estimated. Biomass estimation in this island was done by first classifying the flora growing in the island in four groups, large, medium, small and very small, according to their sizes. For each class, the above ground biomass was estimated by the estimated average height of plants in that class, the estimated average diameter and the surface area occupied. The below ground biomass is estimated as being half of the above ground biomass due to the below ground spread having less area compared to the above ground spread. In Table 5.1, the estimated above ground and below ground biomass in the Henry's island for the three years of 2006, 2009 and 2019 are presented.

Table 5.1: Estimation of biomass in the Henry's island

Above ground biomass, 2006						
Division	Size	Height (H) (m)	Diameter (D) (m^2)	H×D (m^3)	Above ground area (AGA) (m^2)	Above ground biomass (g/m^3)
A	Large	18	5	90	418982	37708380
B	Medium	9	3.26	29.34	566753	16628533.02
C	Small	1.6	1.3	2.08	323774	673449.92
D	Very small	0.3	0.29	0.087	381492	33189.804
Below ground biomass, 2006						
Division	Size	Height (H) (m)	Diameter (D) (m^2)	H×D (m^3)	Below ground area (BGA = AGA / 2) (m^2)	Below ground biomass (g/m^3)
A	Large	18	5	90	209491	18854190
B	Medium	9	3.26	29.34	283376.5	8314266.51
C	Small	1.6	1.3	2.08	161887	336724.96
D	Very small	0.3	0.29	0.087	190746	16594.902
Above ground biomass, 2009						
Division	Size	Height (H) (m)	Diameter (D) (m^2)	H×D (m^3)	Above ground area (AGA) (m^2)	Above ground biomass (g/m^3)
A	Large	18	5	90	179857	16187130
B	Medium	9	3.26	29.34	753741	22114760.94
C	Small	1.6	1.3	2.08	386943	804841.44
D	Very small	0.3	0.29	0.087	60399	5254.713
Below ground biomass, 2009						
Division	Size	Height (H) (m)	Diameter (D) (m^2)	H×D (m^3)	Below ground area (BGA = AGA / 2) (m^2)	Below ground biomass (g/m^3)
A	Large	18	5	90	89928.5	8093565
B	Medium	9	3.26	29.34	376870.5	11057380.47
C	Small	1.6	1.3	2.08	193471.5	402420.72

D	Very small	0.3	0.29	0.087	30199.5	2627.3565
Above ground biomass, 2019						
Division	Size	Height (H) (m)	Diameter (D) (m^2)	H×D (m^3)	Above ground area (AGA) (m^2)	Above ground biomass (g/m^3)
A	Large	18	5	90	764908	68841720
B	Medium	9	3.26	29.34	602999	17691990.66
C	Small	1.6	1.3	2.08	411915	856783.2
D	Very small	0.3	0.29	0.087	232877	20260.299
Below ground biomass, 2019						
Division	Size	Height (H) (m)	Diameter (D) (m^2)	H×D (m^3)	Below ground area (BGA = AGA / 2) (m^2)	Below ground biomass (g/m^3)
A	Large	18	5	90	382454	34420860
B	Medium	9	3.26	29.34	301499.5	8845995.33
C	Small	1.6	1.3	2.08	205957.5	428391.6
D	Very small	0.3	0.29	0.087	116438.5	10130.1495

Table 5.2: Estimation of biomass in the Patibania island

Above ground biomass, 2006						
Division	Size	Height (H) (m)	Diameter (D) (m^2)	H×D (m^3)	Above ground area (AGA) (m^2)	Above ground biomass (g/m^3)
A	Large tree	18	5	90	682211	61398990
B	Small tree	5	3.20	16	583424	9334784
C	Bushes	3	2.80	8.4	328455	2759022
D	Dwarf	0.5	0.25	0.125	123630	15453.75
Below ground biomass, 2006						
Division	Size	Height (H) (m)	Diameter (D) (m^2)	H×D (m^3)	Below ground area (BGA = AGA / 2) (m^2)	Below ground biomass (g/m^3)
A	Large tree	18	5	90	341105.5	30699495
B	Small tree	5	3.20	16	291712	4667392
C	Bushes	3	2.80	8.4	164227.5	1379511
D	Dwarf	0.5	0.25	0.125	61815	7726.875
Above ground biomass, 2009						
Division	Size	Height (H) (m)	Diameter (D) (m^2)	H×D (m^3)	Above ground area (AGA) (m^2)	Above ground biomass (g/m^3)
A	Large tree	18	5	90	628452	56560680
B	Small tree	5	3.20	16	102063	1633008
C	Bushes	3	2.80	8.4	177297	1489294.8
D	Dwarf	0.5	0.25	0.125	1207941	150992.625
Below ground biomass, 2009						
Division	Size	Height (H) (m)	Diameter (D) (m^2)	H×D (m^3)	Below ground area (BGA = AGA / 2) (m^2)	Below ground biomass (g/m^3)
A	Large tree	18	5	90	314226	28280340
B	Small tree	5	3.20	16	51031.5	816504
C	Bushes	3	2.80	8.4	88648.5	744647.4
D	Dwarf	0.5	0.25	0.125	603970.5	75496.3125
Above ground biomass, 2018						

Division	Size	Height (H) (m)	Diameter (D) (m^2)	H×D (m^3)	Above ground area (AGA) (m^2)	Above ground biomass (g/m^3)
A	Large tree	18	5	90	792211	71298990
B	Small tree	5	3.20	16	283994	4543904
C	Bushes	3	2.80	8.4	198478	1667215.2
D	Dwarf	0.5	0.25	0.125	133730	16716.25
Below ground biomass, 2018						
Division	Size	Height (H) (m)	Diameter (D) (m^2)	H×D (m^3)	Below ground area (BGA = AGA / 2) (m^2)	Below ground biomass (g/m^3)
A	Large tree	18	5	90	396105.5	35649495
B	Small tree	5	3.20	16	141997	2271952
C	Bushes	3	2.80	8.4	99239	833607.6
D	Dwarf	1	1.2	1.2	66865	80238

In the Patibania island also, the biomass estimation was carried out in three years, 2006, 2009 and 2018, and estimation was done for both above ground and below ground biomass. However, in the Patibania island, the local plant life was classified in a different collection of four groups, large tree, small tree, bushes and dwarf, because the vegetation characteristics is different compared to the Henry's island. The rest of the estimation procedure is the same as in the case of the Henry's island. The estimated above ground and below ground biomass in the Patibania island are presented in Table 5.2 for the three years of 2006, 2009 and 2018.

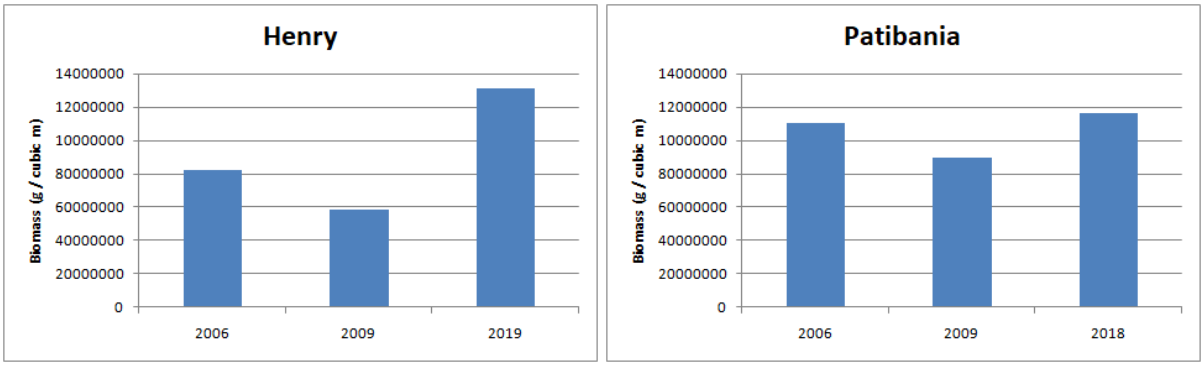

Figure 5.25: Total biomass of the Henry's island and the Patibania island over the years.

The total biomass of an island in a year is estimated by summing the above ground and below ground biomass of the local plant life in all the classes in that island. In Figure 5.25, the bar plots of the estimated total biomass of the two islands are presented across the years. In can be seen from this figure that the total biomass of both the islands declined in 2009 compared to 2006. However, the biomass also recovered later in both the islands to exceed the respective 2006 levels. In the Henry's island, the decline by 2009 was relatively sharper compared to the Patibania island, but its recovery by 2019 is also considerably more prominent than that of the

Plate 5.3: Measuring biomass during fieldwork: measuring height of the tree (top left), diameter measurement of different mangrove species (top right), measurement of areas for the same categories of vegetation (middle left and middle right), measuring above ground biomass (bottom left) and below ground biomass (bottom right).

Patibania island by 2018, and its 2019 biomass significantly exceeds its corresponding level in 2006. In the Patibania island, the decline in total biomass by 2009 was mild, and the 2018 biomass only narrowly exceeds the 2006 level.

The large increase in the biomass of the Henry's island can be explained by the plantation drive undertaken by the forest department and the local community in the aftermath of the supercyclone Aila in 2009, which caused extensive devastation to the local community as well as the mangrove habitats. The mangrove plantation in the Henry's island was carried out to serve as a shield to future cyclones. The dip in the estimated biomass in 2009 can be also explained as the effect of the damages caused by Aila. On the other hand, due to there being no human settlement in the Patibania island, there was no question of human suffering due to cyclonic devastation. So, no such extensive plantation was established there after Aila. The mangroves there recovered naturally, and become only slightly higher in 2019 compared to 2006.

In Plate 5.3, some photos taken during the field excursion for biomass estimation are presented.

5.8 Surface water storage and inundation by tides

There are several water bodies in the islands that store the precipitated rainwater. The areas with lower elevation lying in the intertidal zone gets inundated with saline water during tides. In this section, the surface water storage from rainfall and the saline water influx from tidal inundation are described.

In the Henry's island, the aquacultural ponds occupy a significant portion of the surface area of the island. Rainfall in these ponds are stored as freshwater. There are 5 aquacultural ponds in the island of almost identical surface area. The surface area of a representative pond is measured, and found to be 19061.19 m^2. Thus, the total surface area of all the ponds is 95305.95 m^2. The product of this surface area and the total height of rainfall in a given season is the estimated surface water storage volume in that season in the Henry's island.

In the Patibania island, there are two ponds of nearly identical surface area. The surface area of a representative pond was measured and found to be 1933.5 m^2. So, the total surface area of all ponds in the Patibania island is 3867 m^2. Now, the surface water storage in the Patibania island in a season is estimated in the same way as in the case of the Henry's island by

multiplying this surface area with the total height of rainfall in that season.

Table 5.3: Estimated surface water storage in the two islands (m^3).

Year	Henry's island			Patibania island		
	Pre-monsoon	Monsoon	Post-monsoon	Pre-monsoon	Monsoon	Post-monsoon
2000	55837.37	136604.91	33557.99	2265.58	5542.69	1361.60
2001	63281.70	108420.05	20715.09	2567.63	4399.10	840.51
2002	87140.52	125295.78	42507.81	3535.69	5083.82	1724.74
2003	61876.78	169503.69	24416.67	2510.62	6877.54	990.70
2004	53919.73	154598.88	15462.99	2187.77	6272.79	627.40
2005	58590.56	165609.41	46418.27	2377.29	6719.53	1883.40
2006	52820.19	180101.10	12385.48	2143.16	7307.53	502.54
2007	27000.18	175765.60	13450.34	1095.52	7131.62	545.74
2008	21167.19	102567.15	25046.40	858.85	4161.62	1016.25
2009	33595.35	117760.03	1124.61	1363.12	4778.07	45.63
2010	25189.36	79199.24	3840.83	1022.05	3213.48	155.84
2011	36143.31	150888.38	8329.74	1466.50	6122.23	337.98
2012	18660.91	119408.82	12751.94	757.16	4844.96	517.40
2013	32165.76	160133.06	13962.32	1305.11	6497.33	566.52
2014	43611.72	93619.03	324.04	1769.53	3798.55	13.15
2015	26132.89	149859.08	4546.09	1060.33	6080.47	184.46
2016	28134.32	132141.70	9806.98	1141.54	5361.60	397.91
2017	18937.29	129301.58	18298.74	768.37	5246.36	742.46
2018	42902.44	138273.18	16858.38	1740.75	5610.38	684.02
2019	52856.68	102253.75	35491.94	2144.64	4148.90	1440.07

From Table 5.3, it can be seen that the estimated surface water storage in the ponds of the Henry's island is far higher than that of the Patibania island. This is due to there being more number of ponds in the Henry's island with far bigger size compared to the Patibania island.

The areas in the two islands lying in the intertidal zones gets inundated in saline water during the tides, and this is one of the major sources of saline water influx in the islands. The method of estimating the total seasonal volume of saline water influx through tidal inundation is described in subsection 1.11.4. The volume of saline water during tidal inundation is not

estimated for each year separately, because tidal heights do not exhibit any significant yearly trend. In Table 5.4, the estimated seasonal tidal inundation volumes in the two islands are presented.

Table 5.4: Estimated tidal inundation volumes in the islands in m^3.

Name of island	Pre-monsoon	Monsoon	Post-monsoon
Henry's island	38727635.28	44837103.56	33954134.71
Patibania island	76435222.55	83154905.97	71467838.07

From Table 5.4, it can be seen that the estimated tidal inundation volumes in the Patibania island is nearly twice of that of the Henry's island. This is due to the extensive depressions present in the Patibania island which get inundated during the tides.

5.9 Groundwater recharge

In the earlier sections, it was demonstrated that rainfall is declining while temperature is rising. Due to the declining nature of freshwater influx and increasing population and human enterprises, the groundwater is utilized more and more in the south-western Sundarban. The rising temperature also causes an increase in the freshwater requirements for human consumption and other activities. Though groundwater recharge occurs from both monsoonal rainfall and percolation of saline water through the ground, groundwater is not completely renewable, especially when if extraction far outweighs the replenishment. Groundwater also provides a degree of protection from land subsidence, and so extracting too much groundwater that depletes the underground reserves may hasten the natural subsidence process of the alluvial deltaic lands of the south-western Sundarban.

The groundwater table is spans a broad area underground of a geographic region, and can be disconnected only through underground hard impermeable geomorphic formations. In the alluvial deposits of Sundarban, such formations are non-existent, and so the groundwater table spans a large area there. As a consequence, the groundwater extracted from a point will affect the groundwater depth in adjacent points. Because the two islands under consideration are so close to each other, their groundwater table and groundwater depth are almost identical. However, this groundwater table is also affected by large amount of extraction from the densely populated Bakkhali area that lies in between the two islands.

Based on the above reasoning, the groundwater depths are obtained from a location near Bakkhali, which is in between the two islands. The data consists of groundwater depth measurements on 28 unevenly spaced dates over the time span from 2008 to 2020. The data is plotted in Figure 5.26. In this plot, one can observe a clear and rapidly rising trend of groundwater depth,

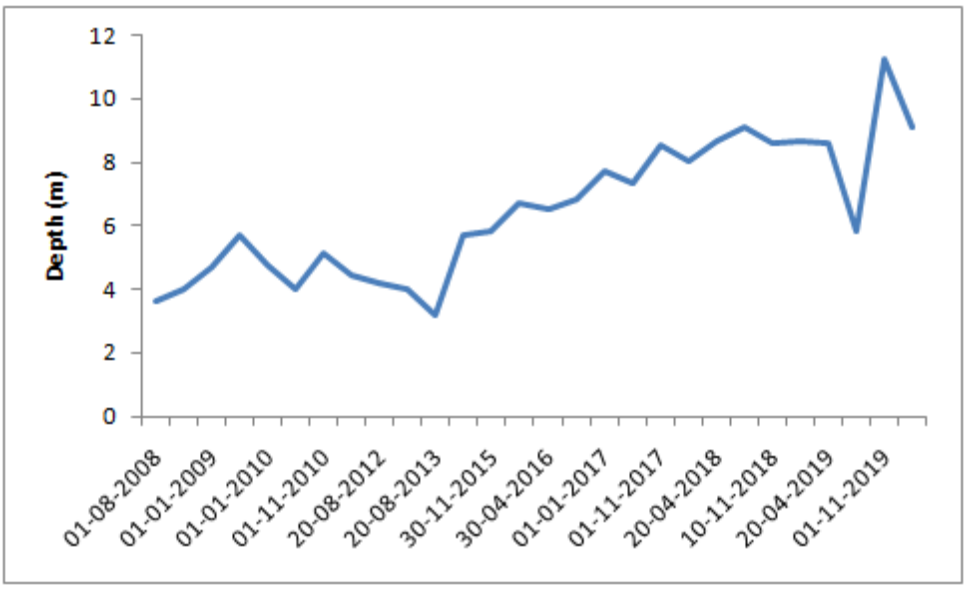

Figure 5.26: Plot of groundwater depth.

with just two notable drops in that depth, one around 2013 and the other around 2019. This trend, along with the numerical value of the groundwater depth, points to an unsustainable rate of extraction of groundwater.

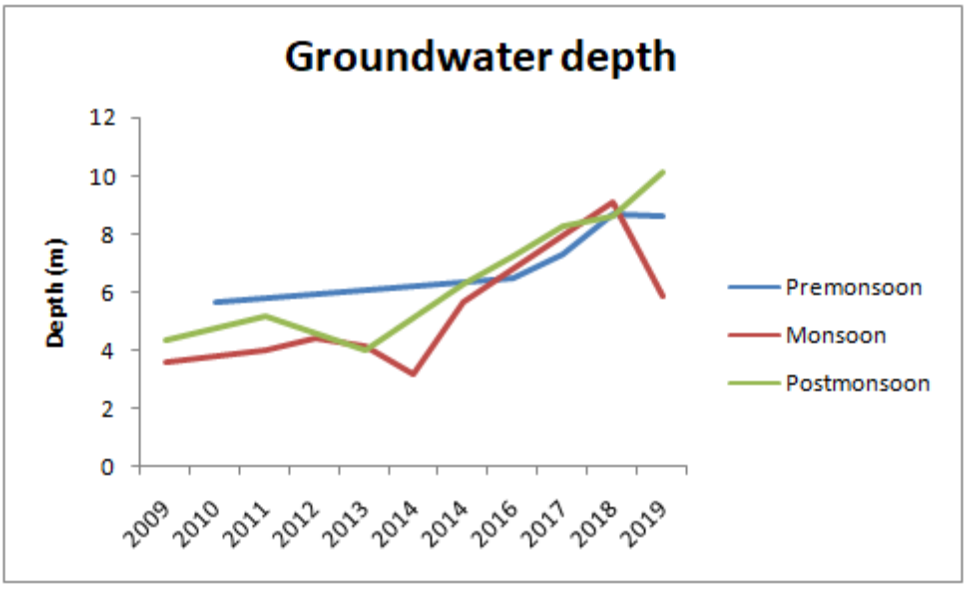

Figure 5.27: Seasonal of groundwater depths (2009–2019).

After making the above observation, one would be interested in looking into the seasonal groundwater dynamics. This is because it is expected a priori that groundwater recharge would occur in the monsoon period with the high levels of rainfall. This recharge should sustain the needs for the post-monsoon and the pre-monsoon period. So, the seasonal values are estimated from the raw data presented in Figure 5.27 over the time period from 2009 to 2019 through linear interpolation. The curves of the estimated seasonal groundwater depths over this period are presented in Figure 5.27. In this plot, one sees that the groundwater depth in all the seasonal are exhibiting increasing trends. The depths in the monsoon and the post-monsoon are lower compared to pre-monsoon till 2014. It is period, almost always the monsoonal depth is lower than that in the post-monsoon. These are along the expected lines, as the groundwater recharge occurring from the monsoonal rainfall decreases the groundwater depth in that season. Groundwater consumption exceeds recharge in the post-monsoon period due to the receding monsoon and resultant decline in rainfall. As summer sets in, freshwater demand rises and the cumulative depletion of groundwater from the previous post-monsoon period shows its effect in the rising depth of groundwater in the pre-monsoon period. However, between 2014 to 2018, a notable feature is reflected in the plot. Here, the monsoon and the post-monsoon depths are higher that the pre-monsoon depth. Also, the rates of increase in groundwater depth in all three seasons in this time period are noticeably higher than the corresponding rates in the previous time span. This indicates a significant decline in groundwater recharge during monsoon in this time period, possibly due to declining rainfall or over-extraction. However, the slightly lower pre-monsoon depth points to significant recharge of groundwater in this time period during the pre-monsoon season, possibly due to atypical weather events bringing a lot of rainfall in the pre-monsoon. However, after 2018, the monsoonal depth again becomes the lowest, indicating to better groundwater recharge. But still the groundwater depths in all three seasons are significantly higher than what they were at the beginning of the time period under consideration.

5.10 Drainage characteristics of the island systems

The drainage systems of the two islands consist of several creeks of varying sizes and man-made canals. These systems serve as the avenues of both inflow and outflow of water in the islands. The eastern side of the Patibania island has higher elevation compared to the western part. The

creek at the eastern boundary of the Patibania island, the Edward's creek, serves as the chief component of the drainage of the Patibania island. On the other hand, the general slope of the Henry's island is from the north to the south. The most important component of the drainage of the Henry's island is the Bakkhali creek.

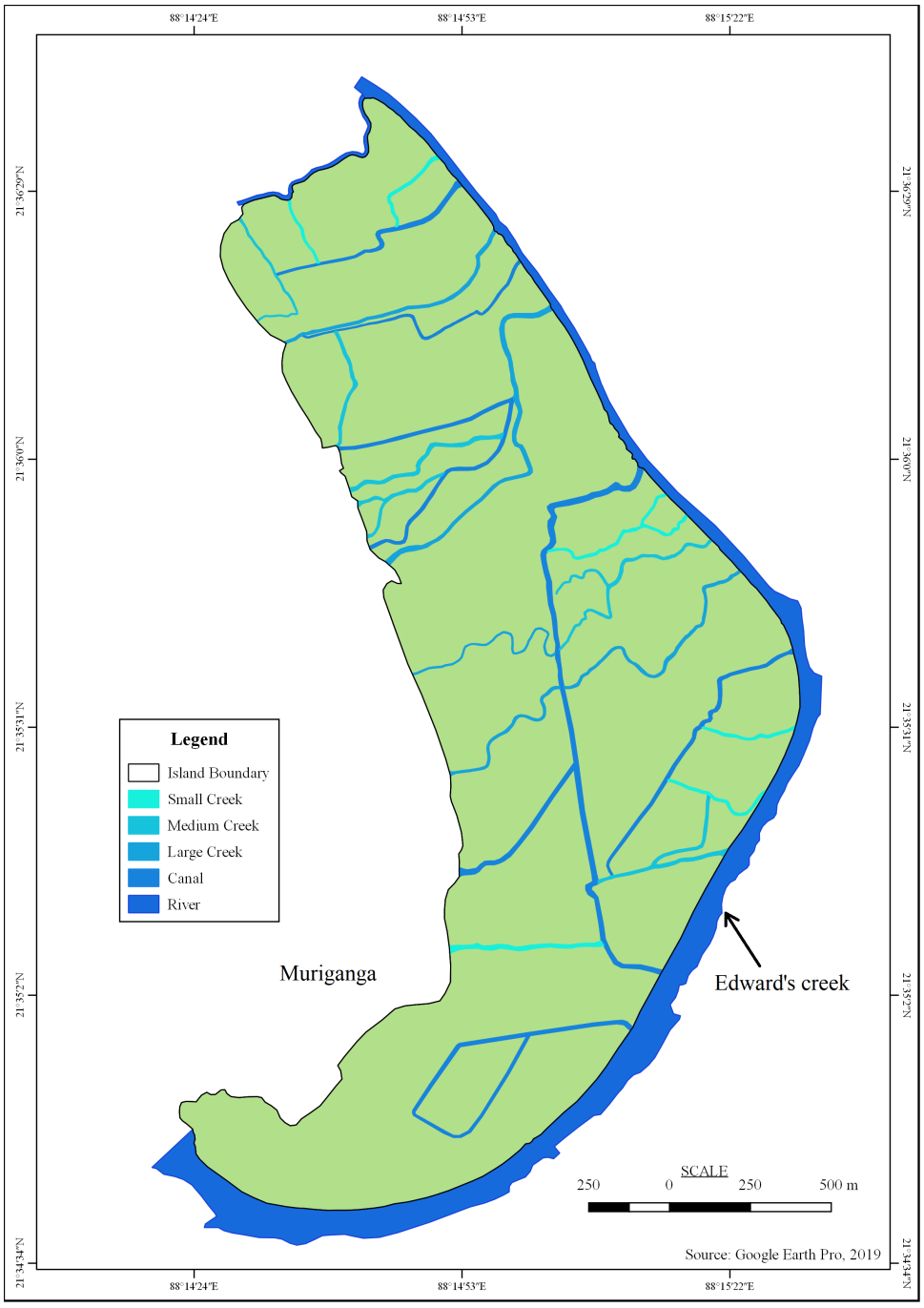

Figure 5.28: Drainage map of the Patibania island.

In Figure 5.28, the drainage map of the Patibania island is presented. It can be observed that due to the east-to-west slope of the island, most of the natural creeks flow from the east to the

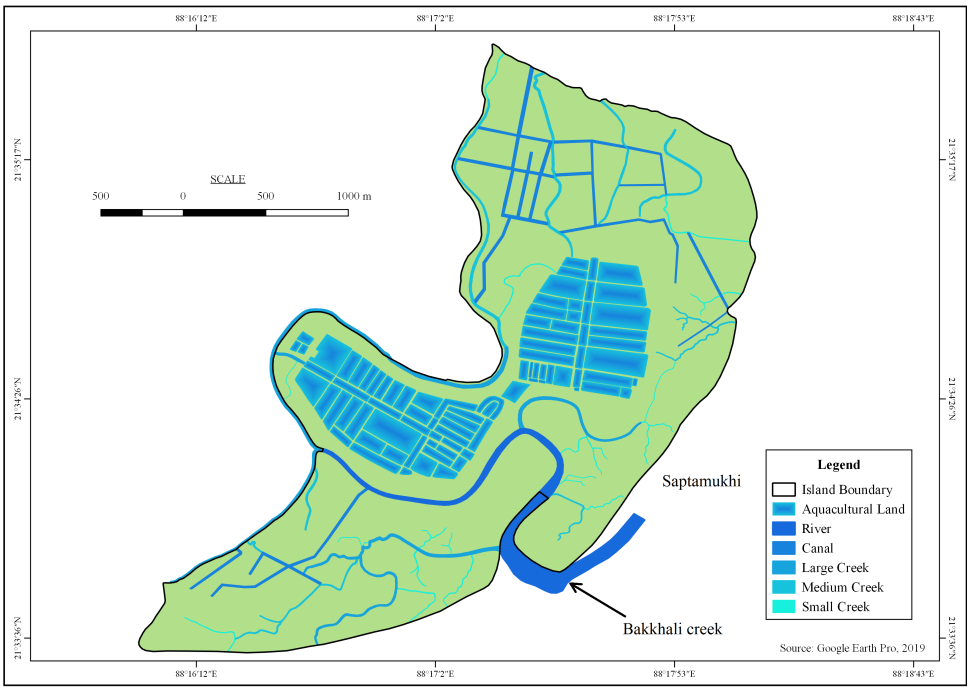

Figure 5.29: Drainage map of the Henry's island.

west and join the sea. The bigger man-made canal however, extends north-south in the central part of the island for a significant portion of its length. The man-made canals were developed to bring water in the inner parts of the island. This additional water inflow is beneficial to the mangrove species growing on the banks of the canals. The drainage network is relatively dense in the northern and the central parts of the islands, and relatively scattered in the middle-north and the southern parts of the island. Though the island has numerous water streams, carrying both saline tidal water and freshwater from the Hooghly estuary, many of the creeks in the island have suffered tidal drainage loss due to siltation. Consequently, their carrying capacity has decreased. The increased elevation of the stream beds has resulted in less water entering through them. As a result, surface water availability in parts of the island has decreased, which adverse affected the vegetation there. At some places, the original paths of the streams have become disconnected due to high siltation, with the upstream portions being lost over time due to the tidal water-fed nature of the streams.

The drainage map of the Henry's island is presented in Figure 5.29. The general slope of the island is from the north-west to the south-east and the east. It can be observed that most of the creeks joining the sea or the Saptamukhi estuary flow in those directions. The principle component of the drainage system is the Bakkhali creek, which meanders through the central and the southern parts of the island and join the Bay of Bengal forming a wide mouth. Several

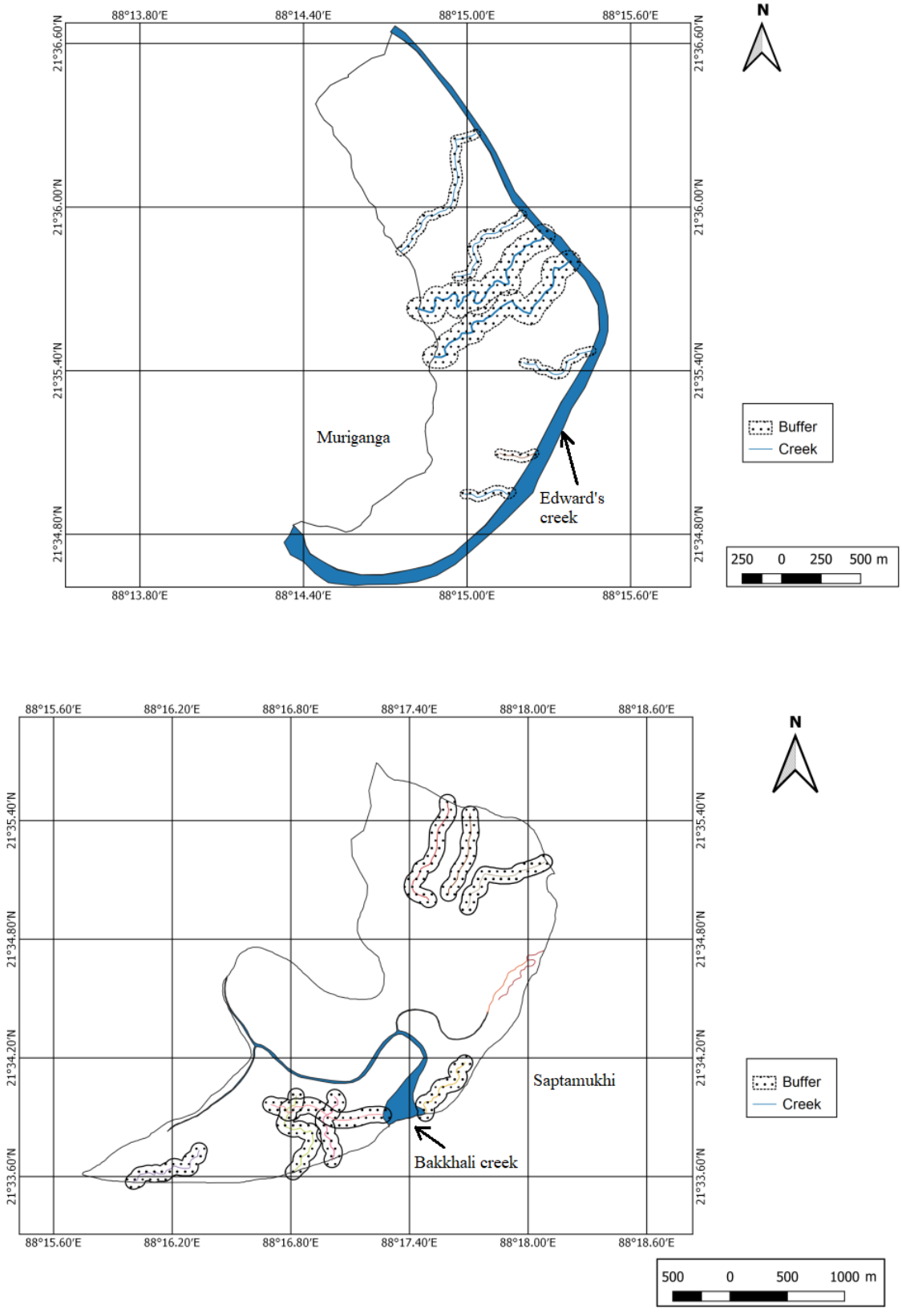

Figure 5.30: Buffer region of the larger creeks in the two islands.

smaller creeks reaching the central and the southern parts of the island have branched out from the Bakkhali creek. Many of these creeks have become beheaded from their main sources due to blocking of the channels. The man-made canals are spread over the northern region of the island, with a few flowing in the southern part. The canals form a relatively dense network in the north. Unlike the Patibania island, the Henry's island has aquacultural enterprises, and the aquacultural ponds situated in the central part of the island are salient parts of the surface water drainage and storage in the island. Like the Patibania island, the streams in the Henry's island also suffered from tidal drainage loss. The decline in water availability inland played its part in the generation of saltpan areas there.

In Figure 5.30, the buffer regions of some of the creeks in the Patibania island and the Henry's island are displayed. The buffer regions for the larger creeks cover regions within the distance of 75 m on either side of the creeks, while for the smaller creeks, the buffer regions cover 50 m on either side of the creeks. The closer a region is to a creek, the higher is the moisture level in the soil of that region. As one moves away from the creeks, the moisture level in the soil decreases. In the buffer regions displayed in Figure 5.30, the moisture level in soil is high, which makes the regions suitable for the growth of the larger mangrove trees. In regions away from the creeks beyond the buffer regions, the low moisture level in soil is associated with salinization. In regions with very high salinity in soil, saltpans develop. No saltpan is observed in the buffer regions displayed in Figure 5.30. The size of the saltpans are larger as one moves away from the buffer regions.

5.11 Assessment of tidal prism in the islands

Tidal prism is the volume water that enters a basin in between the lowest point of the low tide till the highest point of the high tide. Thus, it can be estimated by the product of the basin surface area and the tidal range in that basin. Tidal prism is a major source of saline water influx in the coastal areas. It enters inland through the estuaries and creeks in coast. The Henry's island and the Patibania island both have several creeks, some of which flow along their boundaries and others spread deep inland. These are the chief avenues of saline water intake in the islands under study, and far outweigh the other major source of saline water ingress in the islands, which is tidal inundation of land areas.

The method of tidal prism estimation for each tidal cycle, then the estimation of daily and

Table 5.5: Estimated seasonal tidal prism in the islands (m^3).

Estimated seasonal tidal prism in Henry's island (m^3)						
Type	Number	Length (m)	Width (m)	Pre-monsoon (m^3)	Monsoon (m^3)	Post-monsoon (m^3)
Large	1	7661	32	185884052.48	195864190.40	178627553.28
Medium	2	2069	10.4	32631010.05	34382973.04	31357168.13
Small	4	830	2.25	5664052.80	5968156.50	5442940.80
Total tidal prism (m^3)				224179115.33	236215319.94	215427662.21
Estimated seasonal tidal prism in Patibania island (m^3)						
Type	Number	Length (m)	Width (m)	Pre-monsoon (m^3)	Monsoon (m^3)	Post-monsoon (m^3)
Large	1	5510	32	133692876.80	140870864.00	128473804.80
Medium	1	2050	10.4	16165676.80	17033614.00	15534604.80
Small	3	800	2.25	4094496.00	4314330.00	3934656.00
Total tidal prism (m^3)				153953049.60	162218808.00	147943065.60

seasonal tidal prism volumes are described in subsection 1.11.4. Here, the estimated tidal prism volumes for the three season in both the islands are presented in Table 5.5.

Plate 5.4: Measuring tidal prism in a large creek.

Because the tidal forces exhibits only short term trend which get contained within the seasons, the estimation of tidal prism volumes are not required separately for every year.

From Table 5.5, it can be seen that the Henry's island has relatively higher tidal prism volume owing to its larger creeks. The tidal prism volumes are also substantial, as expected.

5.12 Human consumption of freshwater in the islands

Human consumption is a principal component of the 'artificial' consumption of freshwater in the islands. Here 'artificial' points to consumption of freshwater by entities other than the local flora and natural hydrological processes. Although in this class of artificial consumption of freshwater, human economic activities constitute a far larger proportion, direct human consumption of water for biological and hygienic needs is considerably larger than the consumption by other animals. Moreover, human requirements are the most important from the management angle, as humans alter and shape the geomorphology of the islands and exploit the hydrological processes to fulfill their needs.

Recall that the Henry's island contain significant human activities while the Patibania island is off limits to most human ventures owing to it being a reserve forest. So, the Henry's island sees a large human footfall compared to the Patibania island, which also varies with the seasons due to the seasonal fluctuation of tourism. The Patibania island has one small forest department post manned by only two employees. On the other hand, it is estimated that in the Henry's island, in the pre-monsoon season there are on average 50 humans present daily, in the monsoon season the daily human presence slightly drops to 45 due to the monsoons hindering tourism activities, and then in the post-monsoon the daily human presence increases to 60 due to this seasons being the peak tourism season. It is estimated that an average human utilizes 90 liters (i.e., 0.09 m^3) of water daily for personal uses. Thus, in a season, the total daily human consumption in cubic meter is estimated by multiplying 0.09 to the average daily human presence in that season. Due to the seasonal variation of human presence in the Henry's island, the estimated total daily human consumption in that island varies across the seasons, while the one at the Patibania island remains constant over the seasons.

Next, to obtain the total seasonal human consumption in the islands for each of the seasons, the number of days is multiplied to the estimated total daily human consumption in that island for that season. Recall that the pre-monsoon season is taken to last from February 15 to June

14 consisting of 120 days in a normal year, the monsoon season from June 15 to October 15 consists of 123 days and the post-monsoon season from October 16 to February 14 consists of 122 days. The calculations for the estimation of total seasonal consumption of freshwater by humans is presented in Table 5.6 for both the islands.

Table 5.6: Estimated human consumption of freshwater in the Henry's island

Human consumption	Pre-monsoon	Monsoon	Post-monsoon
Consumption per day per individual (liter): 90 Consumption per day per individual (m^3): 0.09			
Estimation of human consumption of freshwater in the Henry's island			
Number of individuals in season	50	45	60
Number of days in season	120	123	122
Total consumption in season (m^3)	540	498.15	658.8
Estimation of human consumption of freshwater in the Patibania island			
Number of individuals in season	2	2	2
Number of days in season	120	123	122
Total consumption in season (m^3)	21.6	22.14	21.96

In Table 5.6, it can be found that the post-monsoon consumption is highest in the Henry's island due to the higher number of humans present daily owing to the tourist season, while the monsoon consumption is highest in the Patibania island because it consists of the maximum number of days.

5.13 Assessment of the water budget and mangrove ecosystem services in the islands

In this section, the seasonal breakdown of the estimated freshwater and saline water availability after consumption from natural hydrological processes and consumption through human activities and consumption by animals is presented. Recall the description of the hydrological model given in subsection 1.11.4. Recall that the source of freshwater in the islands includes rainfall and groundwater (when groundwater depth increases), the source of saline water includes tidal inundation of the islands, tidal prism and storm surges associated with cyclones. The artificial

consumption, which is defined as consumption of water in human activities and by animals, is involved in exclusively freshwater consumption. Other processes, including surface runoff, channel runoff, throughflow and evaporation consume both freshwater and saline water. If the groundwater table rises in a season, it means groundwater table recharge has acted as a consumption point for both freshwater and saline water. After subtracting the freshwater and saline water consumption from the respective water available, the remaining freshwater and saline water are estimated.

To gauge the changes in the water budget over time, two years are chosen: 2010 and 2019. In Table 5.7 and Table 5.8, the water balance calculations are presented for the years 2010 and 2019, respectively, in the Henry's island. Next, the water balance calculations for the Patibania island are presented in Table 5.7 and Table 5.8, for the years 2010 and 2019, respectively.

Table 5.7: Estimation of water budget available in 2010 in the Henry's island (m^3).

	Type	Source	Pre-monsoon	Monsoon	Post-monsoon
Freshwater	Source	Rainfall	1218423.00	3830910.00	185783.00
Freshwater	Net source	Groundwater	322700.00	0.00	5163200.00
Total freshwater supply			1541123.00	3830910.00	5348983.00
Saline water	Source	Tidal inundation	38727635.28	44837103.56	33954134.71
Saline water	Source	Tidal prism	224179115.33	236215319.94	215427662.21
Saline water	Source	Cyclone surge	0.00	0.00	0.00
Total saline water supply			262906750.61	281052423.50	249381796.92
Total water supply			264447873.61	284883333.50	254730779.92
Freshwater proportion			0.005828	0.013447	0.020999
Saline water proportion			0.994172	0.986553	0.979001
Freshwater	Consumption	Artificial	216359.38	79715.97	195129.95
Freshwater	Consumption	Surface runoff	365526.90	1149273.00	55734.90
Combined	Consumption	Channel runoff	149432947.20	153168770.88	151923496.32
Combined	Consumption	Throughflow	2187932.88	2242631.20	2224398.43
Combined	Consumption	Evaporation	2544790.52	1979284.68	1319591.17
Combined	Net consumption	Groundwater	0.00	3365300.00	0.00
Total natural consumption			154531197.50	161905259.76	155523220.82
Total water consumption			154747556.88	161984975.73	155718350.77
Net available			109700316.73	122898357.77	99012429.15
Net freshwater available			639300.59	1652650.37	2079119.77
Net saline water available			109061016.14	121245707.40	96933309.38

Table 5.8: Estimation of water budget available in 2019 in the Henry's island (m^3).

	Type	Source	Pre-monsoon	Monsoon	Post-monsoon
Freshwater	Source	Rainfall	2556706.00	4946069.00	1716764.00
Freshwater	Net source	Groundwater	0.00	0.00	14982500.00
Total freshwater supply			2556706.00	4946069.00	16699264.00

Saline water	Source	Tidal inundation	38727635.28	44837103.56	33954134.71
Saline water	Source	Tidal prism	224179115.33	236215319.94	215427662.21
Saline water	Source	Cyclone surge	213794.49	0.00	213794.49
Total saline water supply			263120545.10	281052423.50	249595591.41
Total water supply			265677251.10	285998492.50	266294855.41
Freshwater proportion			0.009623	0.017294	0.062710
Saline water proportion			0.990377	0.982706	0.937290
Freshwater	Consumption	Artificial	244026.70	102770.48	226781.06
Freshwater	Consumption	Surface runoff	767011.80	1483820.70	515029.20
Combined	Consumption	Channel runoff	149432947.20	153168770.88	151923496.32
Combined	Consumption	Throughflow	2003913.01	2054010.83	2037311.56
Combined	Consumption	Evaporation	3440125.99	2385866.78	1085877.21
Combined	Net consumption	Groundwater	322700.00	12677500.00	0.00
Total natural consumption			155966698.00	171769969.19	155561714.28
Total water consumption			156210724.70	171872739.67	155788495.34
Net available			109466526.40	114125752.83	110506360.07
Net freshwater available			1053435.04	1973695.19	6929817.99
Net saline water available			108413091.37	112152057.64	103576542.08

Table 5.9: Estimation of water budget available in 2010 in the Patibania island (m^3).

	Type	Source	Pre-monsoon	Monsoon	Post-monsoon
Freshwater	Source	Rainfall	803472.00	2526240.00	122512.00
Freshwater	Net source	Groundwater	212800.00	0.00	3404800.00
Total freshwater supply			1016272.00	2526240.00	3527312.00
Saline water	Source	Tidal inundation	76435222.55	83154905.97	71467838.07
Saline water	Source	Tidal prism	153953049.60	162218808.00	147943065.60
Saline water	Source	Cyclone surge	0.00	0.00	0.00
Total saline water supply			230388272.15	245373713.97	219410903.67
Total water supply			231404544.15	247899953.97	222938215.67
Freshwater proportion			0.004392	0.010191	0.015822
Saline water proportion			0.995608	0.989809	0.984178
Freshwater	Consumption	Artificial	1052.89	3245.09	187.19
Freshwater	Consumption	Surface runoff	241041.60	757872.00	36753.60
Combined	Consumption	Channel runoff	139898534.40	143395997.76	142230176.64
Combined	Consumption	Throughflow	1327537.61	1360726.05	1349663.23
Combined	Consumption	Evaporation	1678126.50	1305211.59	870185.94
Combined	Net consumption	Groundwater	0.00	2219200.00	0.00
Total natural consumption			143145240.11	149039007.40	144486779.41
Total water consumption			143146293.00	149042252.48	144486966.60
Net available			88258251.15	98857701.49	78451249.07
Net freshwater available			387608.59	1007415.60	1241249.87
Net saline water available			87870642.56	97850285.89	77209999.19

Table 5.10: Estimation of water budget available in 2019 in the Patibania island (m^3).

	Type	Source	Pre-monsoon	Monsoon	Post-monsoon

Freshwater	Source	Rainfall	1685984.00	3261616.00	1132096.00
Freshwater	Net source	Groundwater	0.00	0.00	9880000.00
Total freshwater supply			1685984.00	3261616.00	11012096.00
Saline water	Source	Tidal inundation	76435222.55	83154905.97	71467838.07
Saline water	Source	Tidal prism	153953049.60	162218808.00	147943065.60
Saline water	Source	Cyclone surge	406633.80	0.00	406633.80
Total saline water supply			230794905.95	245373713.97	219817537.47
Total water supply			232480889.95	248635329.97	230829633.47
Freshwater proportion			0.007252	0.013118	0.047707
Saline water proportion			0.992748	0.986882	0.952293
Freshwater	Consumption	Artificial	2175.48	4180.52	1471.42
Freshwater	Consumption	Surface runoff	505795.20	978484.80	339628.80
Combined	Consumption	Channel runoff	139898534.40	143395997.76	142230176.64
Combined	Consumption	Throughflow	1241196.26	1272226.17	1261882.87
Combined	Consumption	Evaporation	2268542.95	1573326.47	716066.53
Combined	Net consumption	Groundwater	212800.00	8360000.00	0.00
Total natural consumption			144126868.82	155580035.20	144547754.84
Total water consumption			144129044.29	155584215.71	144549226.26
Net available			88351845.65	93051114.26	86280407.21
Net freshwater available			640739.97	1220651.16	4116144.50
Net saline water available			87711105.68	91830463.10	82164262.70

One remarkable observation that can be made from Table 5.7, Table 5.8, Table 5.9 and Table 5.10 is that the freshwater supply is higher in the post-monsoon season than the monsoon in each of the cases. This is occurring due to the enormous amount of groundwater extracted in this season, which even dwarfs the total monsoonal rainfall. Overall, it can be seen that total freshwater available has increased from 2010 to 2019 for each of the seasons and in both islands. However, The enormous amount of groundwater extraction is a cause of concern as it is unsustainable. However, the available freshwater is dwarfed in front of the available saline water. But that is to be expected in a coastal area directly next to the sea.

Based on the overwhelming abundance of saline water compared to freshwater in these islands, it can be concluded that mangrove species which are highly salt tolerant are suitable to grow in these areas. However, in the calculation demonstrated above, the spatial distribution of freshwater and saline water in the islands are not reflected. Areas which are away from the seashore and have relatively higher elevation so as not to be inundated easily in saline water during tides or storm surges, may be suitable for the growth of less salinity tolerant species of mangroves. However, there are also mangrove species which are observed to have higher growth rate with increased salinity, e.g., salinity positively impact the growth of *Avicennia alba* and *Excoecaria agallocha* (Banerjee et al., 2013). *Ceriops decandra* is also found to propagate

favorably in high salinity levels Rahman and Islam (2015). However, the more salinity tolerant species are generally dwarf in nature with less foliage and little or no heartwood. For this reasons, their economic utility is limited. Nevertheless, they act as pioneer mangrove species being the first to colonize a barren tract. In this way, they play a vital role in the ecological succession so that later the climax community can develop. The larger and generally less salinity tolerant mangrove trees have denser foliage and form canopy covers. Their heartwood is also economically important. For example, *Heritiera fomes* is observed to grow well in lower levels of salinity (Rahman and Islam, 2015), and its timber and heartwood is widely used in construction and manufacturing in Sundarban. These species however occur in the climax mangrove communities, found in areas with relatively less salinity levels.